RESEARCH METHODS

Multimodal profiling of atherosclerosis: Protocol and pilot data for the AtherOMICS biobank

Luka Živković[1], Roya Batool[1], Julian Louma[1], Paulo Vinicius Gil Alabarse[1]†, Yingle Li[1], Lanyue Zhang[1], Stefan Mayrhofer[1], Anushree Ray[1], Mohamad Ali Antabi[1], Panagiotis Zangas[1], Jana Mattar[1], Anna Kopczak[1], Andreas Schindler[2], Paul Reidler[3], Yaw Asare[1], Steffen Tiedt[1,4,5], Lars Kellert[4], Abdalla Marei[6], Barbara Rantner[6], Martin Dichgans[1,5,7], Nikolaos Tsilimparis[6], Marios K. Georgakis[1,4,8]*

Copyright © 2026 The Authors, some rights reserved; exclusive licensee American Association for the Advancement of Science. No claim to original U.S. Government Works. Distributed under a Creative Commons Attribution NonCommercial License 4.0 (CC BY-NC).

Omics technologies enable deep profiling of human atherosclerosis but have mostly been applied in small studies lacking integration with other data modalities. AtherOMICS is a biobanking project linking multiomic atherosclerotic plaque phenotyping with blood biobanking, in vivo imaging, and clinical data. Here, we present the study protocol and show pilot results that demonstrate technical feasibility. Since August 2022, 246 patients scheduled to undergo carotid or femoral endarterectomy at Ludwig-Maximilians-Universität Klinikum (Munich, Germany), have been enrolled (median age, 73 years; 32% female), with recruitment ongoing. Plaques undergo systematic histological characterization of lipid core, calcification, intraplaque hemorrhage, fibrous cap, macrophages, and smooth muscle cells. Single-nucleus RNA sequencing ($n = 17$) has confirmed macrophages as the dominant intraplaque cell type, whereas paired plaque and plasma affinity–based proteomics ($n = 88$) quantified 2841 shared proteins showing low plaque-plasma correlation (median $\rho = 0.10$). Cross-modality image integration [histology, ex vivo magnetic resonance imaging (MRI), in vivo MRI, and computed tomography angiography] proved feasible. Together, AtherOMICS enables multimodal characterization of human atherosclerosis aiming for the discovery of athero-specific drug targets, molecular signatures of atheroprogression, and noninvasive biomarkers of plaque vulnerability.

INTRODUCTION

Atherosclerotic cardiovascular disease (ASCVD) remains the leading cause of mortality and adult disability worldwide (*1*). Despite the widespread adoption of prevention strategies targeting systemic vascular risk factors, the incidence of ASCVD is rising. The destabilization of atherosclerotic plaques is the main mechanism underlying myocardial infarction, ischemic stroke, and cardiovascular death. Decades of research have identified cellular and molecular hallmarks of atheroprogression and plaque destabilization (*2*, *3*), which could reveal novel therapeutic targets, as evidenced by the development of anti-inflammatory atheroprotective strategies for the prevention of ischemic stroke and myocardial infarction (*4*–*6*). However, the mechanisms driving atheroprogression in humans remain underexplored (*7*, *8*). Most mechanistic studies leverage animal models of atherosclerosis, which often fail to translate to humans (*9*). For instance, different genetic underpinnings in murine and human atheroprogression result in differential plaque compositions and an absence of plaque rupture in mice, highlighting the need to prioritize the use of human biomaterials in atherosclerosis research (*10*, *11*). Current concepts of human atheroprogression are largely informed by histopathological studies conducted in the 1960s and 1970s (*12*, *13*). Since then, advances in biotechnology have uncovered previously unknown molecular regulators of atheroprogression (*14*–*17*). Deep multiomics profiling could offer an avenue for dissecting these mechanisms and informing future trials (*18*, *19*).

Beyond targeting systemic risk factors, current guidelines for the prevention and treatment of ischemic stroke, acute coronary syndrome, and peripheral artery disease include endovascular and surgical treatments that carry inherent periprocedural risks. Advancing pharmacotherapies that target plaque biology, however, requires diagnostic and risk stratification tools capable of capturing local plaque progression (*20*). While best practices emphasize the need for personalized risk assessment, existing risk estimators build on systemic cardiovascular risk factors rather than plaque progression biomarkers (*21*). Ultrasonography, computed tomography angiography (CTA), and magnetic resonance imaging (MRI) are noninvasive diagnostics that can reliably identify atherosclerotic plaques and assess basic composition features (*22*). Similarly, omics technologies could help detect circulating signatures of plaque destabilization (*17*) for targeted therapies and treatment response monitoring (*23*). Nevertheless, efforts to link in vivo imaging and circulating molecular signatures with extensive phenotyping of the plaque microenvironment remain limited (*24*).

To address these gaps, we have launched AtherOMICS, a biobanking study that integrates deep phenotyping of human atherosclerotic plaques with peripheral blood biobanking, multimodal in vivo noninvasive imaging, and clinical data collection (Fig. 1). We perform extensive histopathological and omics analyses in plaque samples from patients undergoing carotid or femoral endarterectomy and integrate the derived data with matched preoperative blood samples and in vivo plaque imaging. The objectives of AtherOMICS

[1]Institute for Stroke and Dementia Research (ISD), University Hospital, LMU Munich, Munich, Germany. [2]Institute of Neuroradiology, University Hospital, LMU Munich, Munich, Germany. [3]Department of Radiology, University Hospital, LMU Munich, Munich, Germany. [4]Department of Neurology, University Hospital, LMU Munich, Munich, Germany. [5]Munich Cluster for Systems Neurology (SyNergy), Munich, Germany. [6]Department of Vascular Surgery, University Hospital, LMU Munich, Munich, Germany. [7]German Centre for Neurodegenerative Diseases (DZNE), Munich, Germany. [8]Program in Medical and Population Genetics and Cardiovascular Disease Initiative, Broad Institute of MIT and Harvard, Cambridge, MA, USA.
*Corresponding author. Email: marios.georgakis@med.uni-muenchen.de
†Present address: Institute for Clinical Chemistry and Laboratory Medicine, UKE Hamburg, Hamburg, Germany.

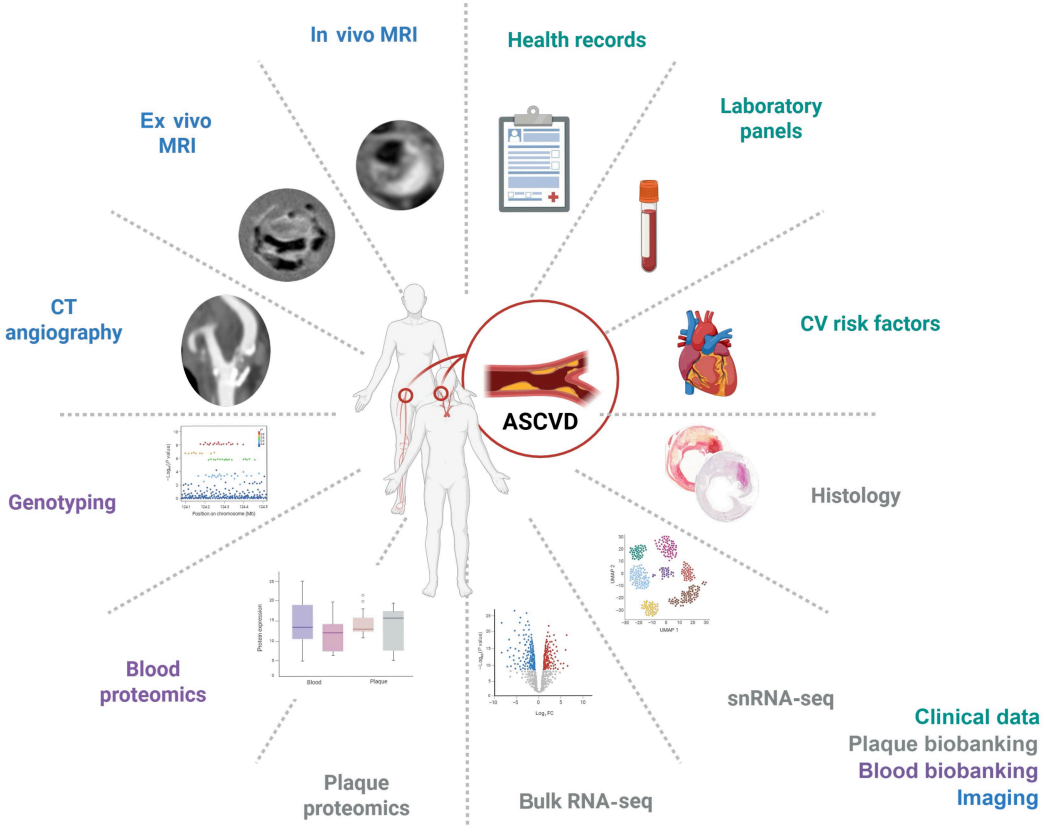


Fig. 1. Schematic overview of AtherOMICS data types. CV, cardiovascular; CT, computed tomography. The representative image for "ex vivo MRI" is also shown in Fig. 5B. Created in BioRender. L. Bernhagen (2026) https://BioRender.com/0naerqx.

are to (i) identify druggable molecular mechanisms driving plaque progression, (ii) detect molecular signatures of plaque destabilization, and (iii) develop a multimodal biomarker panel of plaque vulnerability. Here, we present the study protocol including detailed methods for participant recruitment, biosample collection and processing, clinical data extraction, and imaging. In addition, we show pilot results from our standardized plaque histology assessments, multiomics profiling, and multimodal plaque imaging.

RESULTS

Patient cohort

As of 16 November 2025, 246 patients were recruited to the AtherOMICS biobank (Fig. 2). Recruitment started in August 2022 with patients undergoing carotid endarterectomy and was expanded in March 2024 to include patients undergoing femoral endarterectomy (fig. S1A). Of the participants, 212 underwent carotid endarterectomy for either asymptomatic (38.2%) or symptomatic (61.8%) carotid stenosis, while 34 patients underwent femoral endarterectomy for advanced peripheral artery disease. Among patients with symptomatic carotid stenosis, the most common qualifying event was ischemic stroke (48.9%), followed by transient ischemic attack (24.4%), amaurosis fugax (12.2%), and central retinal artery occlusion (8.3%) (fig. S1B).

Baseline characteristics of patients undergoing carotid endarterectomy are summarized in Table 1. As expected, there was a high prevalence of vascular risk factors with 77, 69, and 25% reporting a history of hypertension, hypercholesterolemia, or diabetes, respectively. Furthermore, 35, 26, and 16% of the patients undergoing carotid endarterectomy had a history of coronary artery disease, prior stroke, or peripheral artery disease, respectively. Baseline characteristics of the recruited patients undergoing femoral endarterectomy are presented in table S1.

Histopathological plaque characterization

Collected plaques undergo initial processing until flash-freezing within a median of 40 [interquartile range (IQR), 33 to 50] min after removal (fig. S1C). All excised plaques undergo ex vivo MRI and histological assessment for morphological characterization (Fig. 3A). Initial quantifications of plaque macrophage and smooth muscle cell content reveal no statistically significant differences between symptomatic and asymptomatic carotid plaques, noting large variance distributions especially for macrophage content in symptomatic plaques (Fig. 3, B and C). Morphological features, including lipid core size, intraplaque hemorrhage (IPH), calcification, neovessel density, and fibrous cap thickness, are manually segmented and annotated across histological and ex vivo MRI images (Fig. 3, D to I). Across all assessed features, IPH area was significantly larger in plaques from symptomatic patients (asymptomatic: 5.05 ± 11.69% versus symptomatic: 10.02 ± 10.75%, $n = 33$ versus 54, $P = 0.0012$; Fig. 3H). Histological plaque progression grading based on the American Heart Association (AHA) classification indicated a notable shift

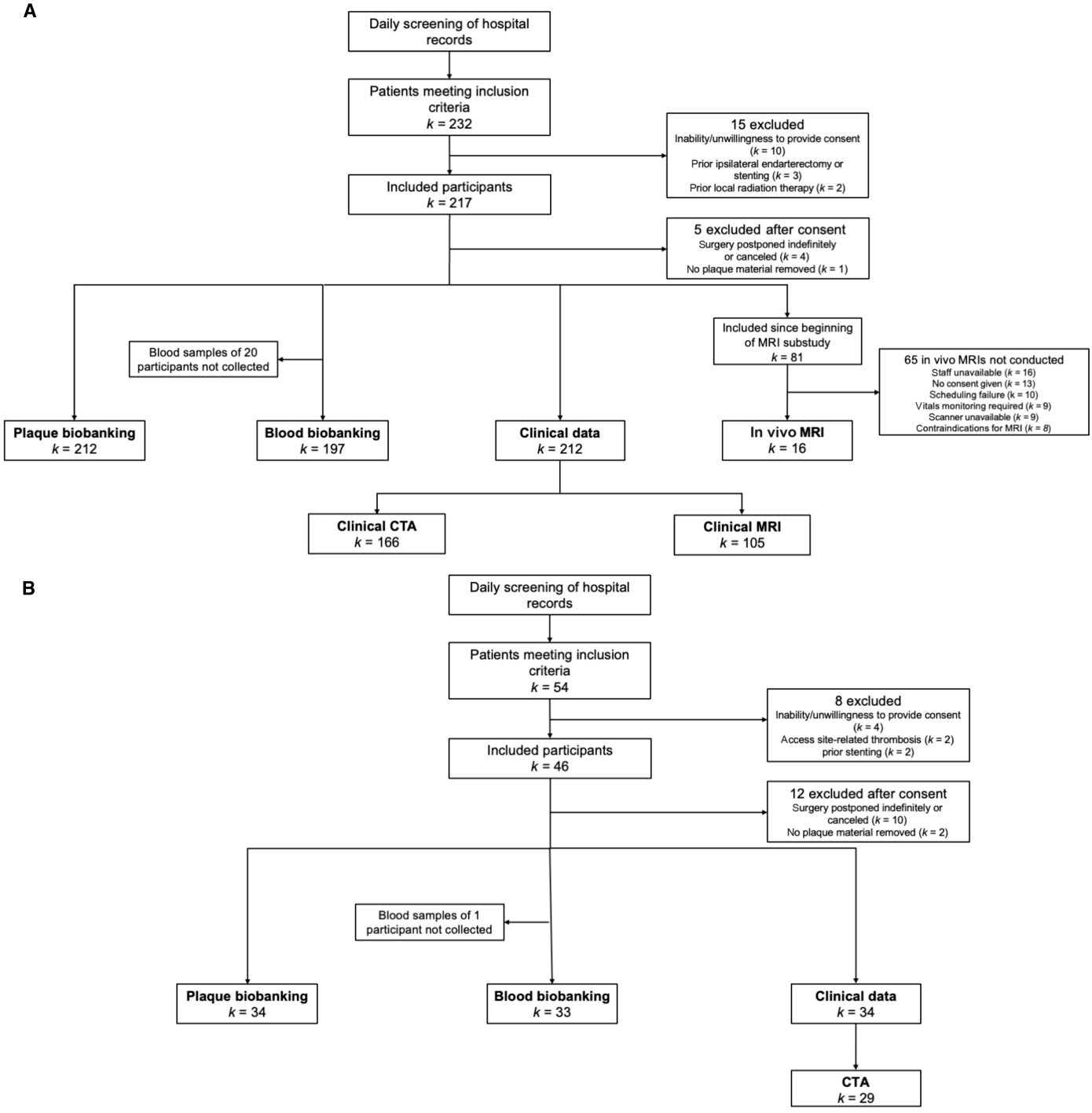


Fig. 2. Study flowchart. Shown is the inclusion process for patients undergoing endarterectomy surgery of either the carotid (**A**) or femoral (**B**) artery.

toward more complicated type VI plaques in symptomatic patients ($P = 0.0003$; table S2).

Proteomics and transcriptomics

Plaque segments and peripheral blood samples (serum and plasma) are stored for omics analyses. To date, we performed single-nucleus RNA sequencing (snRNA-seq) on 17 carotid plaque samples, as well as proximity extension assay proteomics (Olink Explore 3072) for 88 paired carotid plaque and plasma samples. snRNA-seq revealed a total of 19,100 nuclei across the 17 samples, of which 32% were identified as nuclei of macrophages, 29% smooth muscle cells, 14% endothelial cells, 9% T cells, 7% neutrophils, 5% fibroblasts, and 4% plasma cells (Fig. 4A). Our snRNA-seq data point toward macrophages as the predominant immune cell type.

Table 1. Baseline characteristics of recruited patients undergoing carotid endarterectomy in the AtherOMICS study. *P* values are calculated using Pearson's chi-squared test, Welch's two-sample *t* test, or Wilcoxon rank sum test, as appropriate. *P* values highlighted in bold are statistically significant at $\alpha < 0.05$ and a false discovery rate of 0.05 (false discovery rate–adjusted significance threshold, 0.016). MI, myocardial infarction; HbA1c, glycated hemoglobin; BMI, body mass index.

	Overall	Asymptomatic	Symptomatic	*P* value
	***N* = 212**	***N* = 81**	***N* = 131**	
Age (years), median (Q1, Q3)	73 (65, 80)	70 (65, 77)	74 (67, 81)	**0.016**
Females, *n* (%)	68 (32%)	23 (28%)	45 (34%)	0.463
BMI, means ± SD	26.4 ± 4.3	26.9 ± 4.1	26.0 ± 4.5	0.147
Family history of MI or stroke, *n* (%)	105 (50%)	44 (54%)	61 (47%)	0.272
History of hypertension, *n* (%)	163 (77%)	67 (83%)	96 (73%)	0.113
History of diabetes, *n* (%)	52 (25%)	20 (25%)	32 (24%)	0.965
Current smoker, *n* (%)	51 (24%)	14 (17%)	37 (28%)	0.070
History of hypercholesterolemia, *n* (%)	146 (69%)	66 (81%)	80 (61%)	**0.002**
History of coronary artery disease, *n* (%)	75 (35%)	37 (46%)	38 (29%)	**0.014**
History of stroke, *n* (%)	55 (26%)	13 (16%)	42 (32%)	**0.010**
History of peripheral artery disease, *n* (%)	33 (16%)	10 (12%)	23 (18%)	0.309
Antihypertensive medication use, *n* (%)	165 (76%)	66 (80%)	99 (73%)	0.231
Statin use, *n* (%)	155 (71%)	67 (82%)	88 (65%)	**0.009**
Antidiabetic medication use, *n* (%)	50 (23%)	21 (26%)	29 (21%)	0.484
Antiplatelet medication use, *n* (%)	176 (81%)	76 (93%)	100 (74%)	**<0.001**
Total cholesterol (mg/dl), means ± SD	156 ± 40	140 ± 33	165 ± 41	**<0.001**
HDL-C (mg/dl), means ± SD	52 ± 16	55 ± 16	49 ± 15	**0.011**
LDL-C (mg/dl), means ± SD	88 ± 39	70 ± 33	99 ± 38	**<0.001**
HbA1c (%), means ± SD	6.04 ± 0.83	6.11 ± 0.96	6.00 ± 0.74	0.433
CRP (mg/dl), median (Q1, Q3)	0.20 (0.10, 0.50)	0.10 (0.09, 0.30)	0.20 (0.10, 0.60)	**0.003**

Proteomic analysis of 88 matched plaque and plasma samples demonstrated the utility of proximity extension proteomic assays in plaque tissue, revealing the presence of 2841 distinct proteins. The median Spearman correlation between plaque and serum protein levels for these 2841 proteins was $\rho = 0.10$ (IQR, 0.02 to 0.20), although 214 proteins showed a correlation of $\rho > 0.4$ (Fig. 4B). Plasma levels of interleukin-6 (IL-6), a commonly used surrogate of vascular inflammation, were significantly up-regulated in patients with symptomatic compared to asymptomatic plaques ($P < 0.001$; Fig. 4C). There was no significant correlation between plaque and plasma IL-6 levels (Spearman's $\rho = 0.13$, $P = 0.23$, Fig. 4D).

We used transcriptomic and proteomic pilot data to estimate sample size requirements for part of the planned analyses (table S3). For example, we estimated that to detect significant shifts in cell type proportions between symptomatic and asymptomatic plaques, using cell type proportions in the pilot data (*25*), we would need a total sample size of 114 plaques. To detect at least 10 significantly differentially expressed proteins in symptomatic versus asymptomatic plaque tissue, we would require a sample size of 356 plaques (*26*, *27*), whereas for the development of a plasma proteomic biomarker panel composed of 10 proteins that discriminates symptomatic from asymptomatic disease at a *c* index of 0.8, we would need 330 plasma samples (*28*).

Imaging

We collected presurgery head and neck CTA stacks generated in the context of routine diagnostic procedures from 103 patients. In addition, we performed 16 carotid and brain MRI scans as part of the imaging substudy nested within AtherOMICS (Fig. 5), which began imaging participants in August 2024. We noted that plaque features observed in CTA imaging, such as calcification, were also detectable in ex vivo imaging techniques, such as MRI and histology (Fig. 5, A and B). CTA-derived calcification thickness correlated with calcification area quantified in histology (Spearman's $\rho = 0.57$; fig. S4A). We also noted a concordance between CTA-derived soft plaque thickness and histologically derived lipid core area ($\rho = 0.46$; fig. S4B). In vivo MRI performed in the context of the study augmented the characterization of soft plaque tissue in CTA (Fig. 5, C and D). In vivo MRI of 4 symptomatic and 12 asymptomatic patients detected IPH in 9 of 16 carotid arteries (Fig. 5D). The quantification of previously

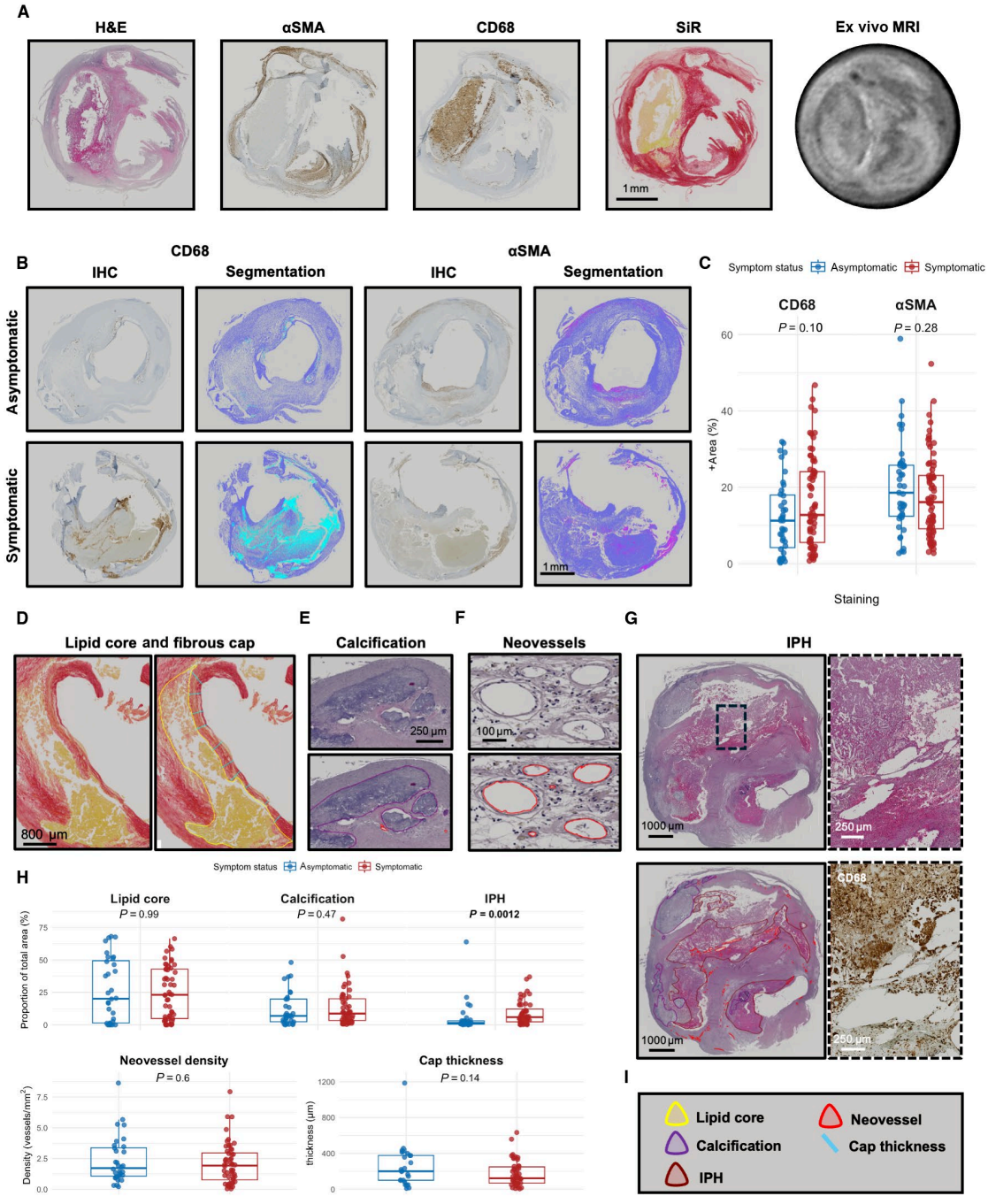


Fig. 3. Histological assessment of carotid atherosclerosis in AtherOMICS. (**A**) Plaque cross section across multiple ex vivo imaging modalities. From left to right: Hematoxylin and eosin (H&E) for general histology, anti–α–smooth muscle actin (αSMA) for smooth muscle cells, anti-CD68 for macrophages, Sirius Red (SiR) for collagen content and lipid cores, and T2*-weighted ex vivo MRI for morphology. Scale bar, 1 mm. (**B**) Quantification of immunohistochemical stainings through automated feature segmentation. Original whole-slide image [immunohistochemistry (IHC)] is displayed next to the result of the segmentation algorithm ("Segmentation" panels). In CD68 segmentation, light-blue indicates positive signal. In αSMA, purple indicates positive signal. Dark-blue indicates negative signal in both stainings. Scale bar, 1 mm. (**C**) Box-and-whisker plot of CD68 and αSMA-positive areas relative to total plaque area in asymptomatic (CD68, $n = 39$; αSMA, $n = 41$) and symptomatic (CD68, $n = 68$; αSMA, $n = 72$) participants. Blue color represents asymptomatic, and red color symptomatic participants. Data points indicate individual values, and the upper and lower boundaries of the boxes indicate Q3 and Q1, respectively. The median is represented through a bold line. Whiskers extend to 1.5× IQR above/below their respective quartiles. *P* values are provided above. Mann-Whitney *U* (CD68) and unpaired, two-sided Student's *t* test (αSMA). (**D** to **G**) Representative images depicting plaque vulnerability features. Bottom panels [(D), right] display examples of manual plaque feature annotation in whole-slide scans before quantification. Scale bars, 800 µm (D), 250 µm (E), 100 µm (F), 1000 µm [(G), left], and 250 µm [(G), right]. (**H**) Box-and-whisker plots comparing plaque vulnerability features in plaques from asymptomatic ($n = 33$) and symptomatic ($n = 54$) participants. *P* values considered statistically significant at $\alpha < 0.05$, and a false discovery rate of 0.05 are provided in bold. Mann-Whitney *U* test. (**I**) Graphical legend for the annotation line colors used in (D) to (G).

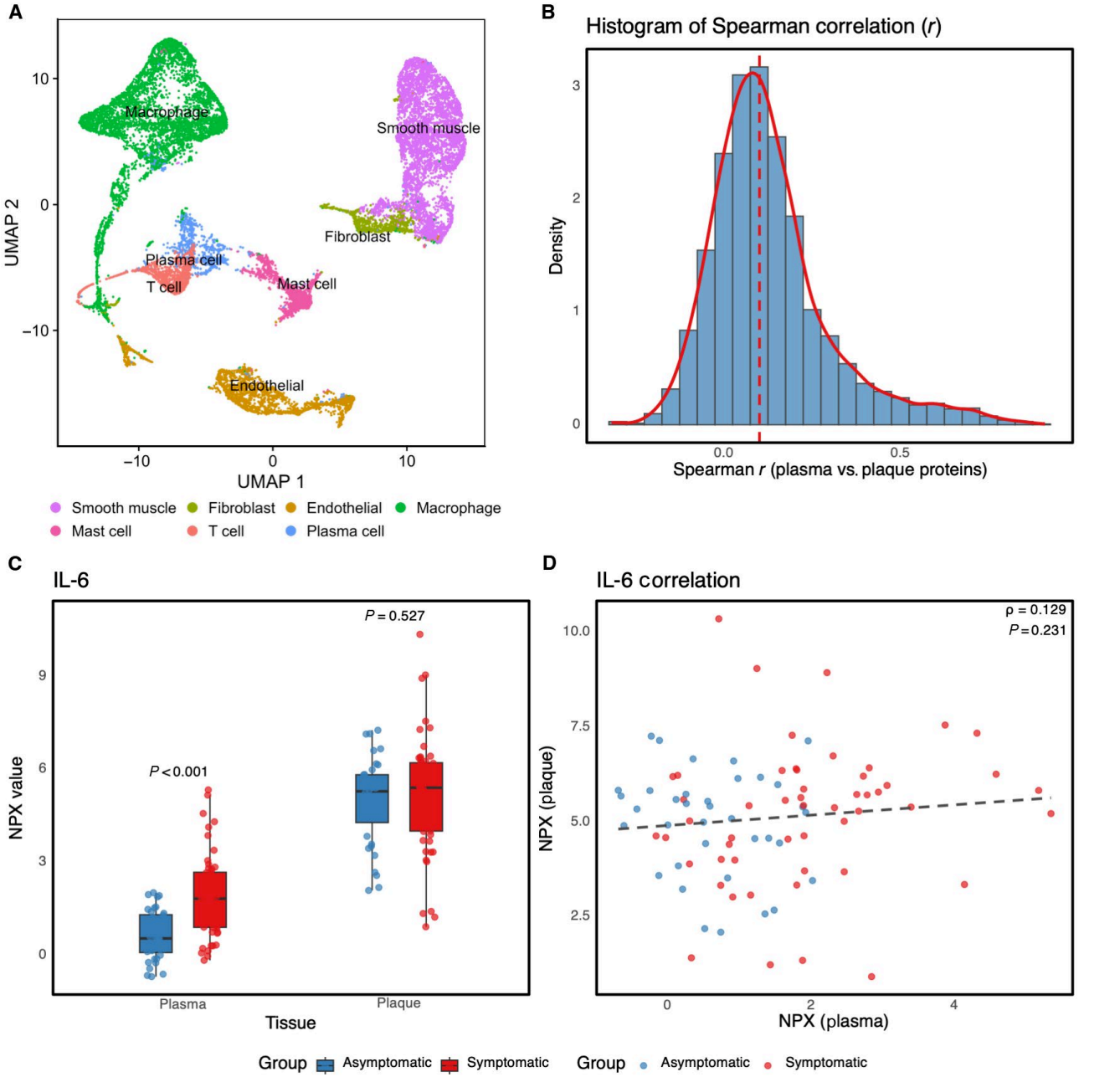


Fig. 4. Single-nucleus transcriptomic and proteomic profiling of plaque and plasma samples from patients undergoing carotid endarterectomy. (**A**) UMAP plot of plaque tissue snRNA-seq data from asymptomatic ($n = 8$) and symptomatic ($n = 9$) participants. (**B**) Histogram and density curve of Spearman correlation coefficients (ρ) between paired plasma and plaque samples computed across 2810 proteins for 88 patients undergoing carotid endarterectomy, overlaid with a density curve. The dashed red line indicates the median correlation coefficient (ρ = 0.10). (**C**) Box plots for plaque and plasma interleukin-6 (IL-6) normalized protein expression (NPX) values in asymptomatic ($n = 37$) and symptomatic ($n = 51$) patients. *P* values are provided above the boxes. Student's *t* test. (**D**) Scatterplot of the plasma and plaque NPX values across the 88 sample pairs.

described, CTA-derived plaque features revealed no significant differences in total plaque thickness and soft plaque thickness at the level of the index lesion, remodeling index, calcification location, and total calcification volume between asymptomatic and symptomatic patients. There was a statistically significant difference in mean calcification density (asymptomatic: 778 ± 317 HU versus symptomatic: 1013 ± 406 HU, $n = 33$ versus 70, $P = 0.001$) (Fig. 5E).

DISCUSSION

Here, we present the study protocol and pilot data from AtherOMICS, a biobanking study of patients undergoing endarterectomy surgery that bridges deep plaque phenotyping with blood biobanking, in vivo noninvasive imaging, and clinical data collection. Our pilot results indicate elevated IPH content in symptomatic plaques, macrophages as the most prevalent immune cell subset in plaque

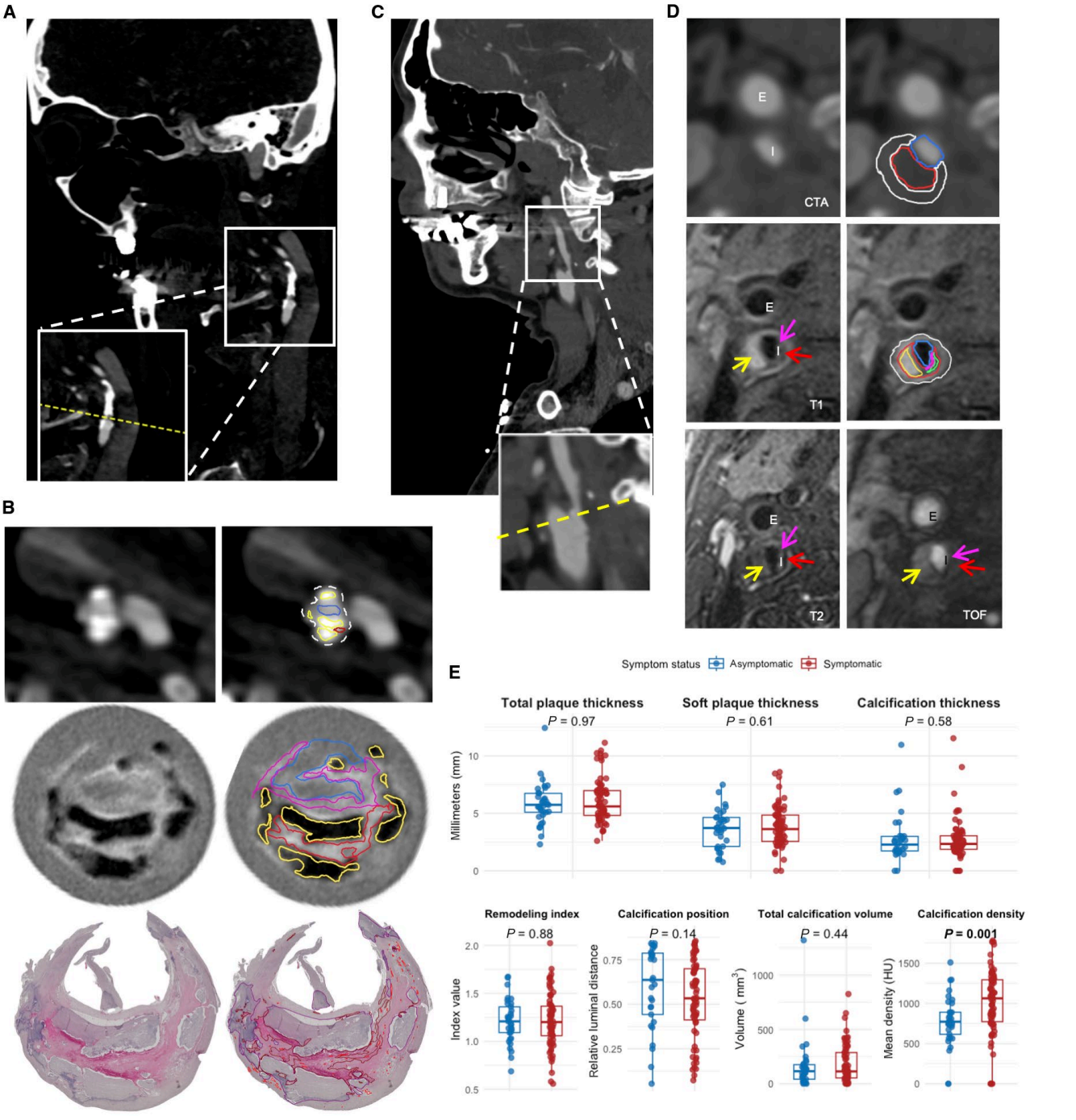


Fig. 5. Multimodal in vivo and ex vivo carotid plaque imaging in AtherOMICS. (**A**) CTA in sagittal plane showing the right carotid artery of a female patient presenting with sudden-onset left upper limb motor deficit before inclusion. The yellow dashed line within the inset indicates the location of the axial plane in (B). (**B**) Presentation of calcification across multiple imaging modalities. Left column displays the original image, and right column displays annotated structures. From top to bottom: Axial-plane CTA, T2-weighted ex vivo MRI, and H&E histology. Annotations: White dashed line denotes outer vessel wall, blue line denotes the lumen, yellow (H&E: purple) line denotes calcification, purple line (H&E: not represented) denotes fibrous cap, and red line denotes soft plaque (H&E: IPH). (**C**) CTA in sagittal plane showing the right carotid artery of a male patient presenting with sudden-onset left upper limb sensorimotor deficit before inclusion. The yellow dashed line within the inset indicates the location of the axial plane in (D). (**D**) Side-by-side comparison of axial CTA and AtherOMICS in vivo MRI imaging. "E" indicates the external carotid artery, and "I" the internal carotid artery. The outer vessel wall is delineated in white, lumen is in blue, soft plaque is in red, IPH and fibrous cap (MRI sequences) are in yellow and purple, respectively. In T1, T2, and time-of-flight (TOF) angiography, the purple arrow points to the fibrous cap, the green arrow points to a lipid core, and the yellow arrow points to IPH on the dorsolateral side of the artery. (**E**) Box-and-whisker plots comparing CTA-derived plaque features in asymptomatic ($n = 29$ to 33) and symptomatic ($n = 69$ to 70) participants. *P* values considered statistically significant at $\alpha < 0.05$, and a false discovery rate of 0.05 are provided in bold (false discovery rate–adjusted significance threshold, 0.007). Student's *t* test (soft plaque thickness and remodeling index) and Mann-Whitney *U* test (all others).

tissue, and an association of IL-6 levels with symptomatic disease, while plasma and plaque proteomic profiles were weakly correlated. We also demonstrate examples of parallel characterization of plaque vulnerability features across histology and multiple imaging modalities. These findings are consistent with prior literature (*29*–*31*) and confirm the technical feasibility of our study. Furthermore, power calculations based on pilot data suggest that sample sizes achievable in this study should provide sufficient power for meaningful discoveries using omics profiling. By integrating these data types, we aim to identify key mechanisms driving plaque progression, understand molecular phenotypes associated with destabilization, and propose noninvasive biomarkers for the detection of vulnerable plaques. AtherOMICS is well positioned to address these goals. To reveal targetable molecules and pathways driving atheroprogression, we first aim to map molecular quantitative trait loci (molQTLs) active within atherosclerotic lesions and link them to genetic loci associated with atherosclerotic cardiovascular outcomes. While hundreds of genomic signals have been detected for cardiovascular disease outcomes in genome-wide association studies (*32*, *33*), underlying mechanisms remain unknown (*34*). Lead variants located in noncoding genomic regions are assumed to influence gene expression; however, functional genomic studies studying tissue-specific expression are lacking (*35*). To this end, we will genotype samples from the AtherOMICS cohort in conjunction with samples from a collaborating study to identify variants associated with molecular plaque features. A recent study of coronary artery tissue and genetic data from 138 participants identified previously unknown expression QTLs associated with ASCVD (*36*). Integrating findings from QTL analysis with existing genomic resources for atherosclerotic traits and end points (*37*) will enable the discovery of specific, genetic drivers of plaque progression and destabilization and reveal druggable downstream targets for subsequent testing in animal models and clinical studies. Previous studies investigating recent drug trial pipelines have suggested that genetic evidence improves the probability of drug targets achieving clinical success (*38*, *39*). Second, we aim to characterize molecular signatures and the underlying pathophysiology of plaque vulnerability. Histopathology has been essential for characterizing atheroprogression, identifying morphological stages of lesion development and substructures linked to plaque vulnerability (*40*, *41*). However, molecular features related to vulnerable plaques remain poorly defined. By linking clinical data and histology with plaque omics profiles, AtherOMICS provides an opportunity to investigate these associations. Third, to find noninvasive diagnostic markers for symptomatic atherosclerotic disease, we will examine how plaque histological and molecular features relate to in vivo imaging phenotypes and to omics profiles in peripheral blood. By aligning imaging and histology data, we aim to characterize how vulnerable plaque substructures appear in noninvasive diagnostics (Fig. 5). In parallel, correlating blood-based omics profiles with plaque features will enable the identification of circulating biomarkers predictive of clinical events such as stroke or myocardial infarction (*42*). Together, these efforts can support the development of noninvasive tools for assessing plaque stability and forecasting adverse cardiovascular outcomes.

Initial quantification of histological plaque vulnerability features in AtherOMICS tissue sections indicates that IPH content is increased in symptomatic carotid plaques. IPH is regarded as both a driver of plaque destabilization and an indicator of complicated plaques (*29*, *43*, *44*). Histopathological studies using carotid endarterectomy samples from the AtheroExpress biobank (*45*) and coronary autopsy samples (*46*) have developed the understanding that leakage from intraplaque neovessels is a causal mechanism for IPH. Recently, multiple studies integrating transcriptomic data at the single-cell, bulk, and spatial level from the MaasHPS study (*47*) and the Munich Vascular Biobank (*48*) identified distinct neovessel-adjacent endothelial cell subpopulations in vulnerable plaques. Another study incorporating carotid plaque proteomics and multiomic characterization of extracellular vesicles highlighted cell-cell communication between endothelial cells dominated by neovascularization-associated molecules in vulnerable plaques (*49*). One proteomic and transcriptomic analysis of carotid plaque tissue and peripheral plasma from the BiKE study proposed Biliverdin reductase B as a biomarker associating with IPH (*50*). Integrating omics modalities that capture the plaque microenvironment with noninvasive imaging and detailed clinical phenotyping could identify driving mechanisms of plaque microvascular dysfunction and IPH.

Our snRNA-seq data confirms macrophages as the predominant immune cell type in advanced plaques (*30*, *51*). Prior data from single-cell RNA-seq analyses had suggested T cells as the predominant leukocyte subset (*52*, *53*). These diverging results might be related to differences in the viability of immune cell subsets across different protocols (*54*).

Our CTA quantifications exhibited concordance with histology for calcified and soft plaque measurements and a statistically significant increase in mean calcification density in symptomatic plaques, with other variables such as calcification thickness and volume not differing between the two groups. Concurrently, our histological data do not show differences in plaque calcification content. These observations are in line with CTA (*55*) and histopathology (*56*) studies of carotid arteries integrating clinical end points. Future studies on calcification in vascular imaging and histology will shift the focus toward characterization of calcification pattern, fragmentation, position in relation to the lumen, and spatial clustering to identify patient substrata with higher risk of symptomatic conversion (*57*, *58*). Proteomic and transcriptomic profiling of the carotid plaque extracellular matrix revealed a molecular signature for calcified plaques that inversely correlated with plaque inflammation (*59*). A recent study linking carotid plaque histology with bulk sequencing and spatial transcriptomics found a sex-specific difference in the activity of calcification-associated pathways, with fibrous plaques from female patients exhibiting gene expression profiles dominated by extracellular remodeling that mapped to distinct plaque regions (*60*). Subtyping calcification in histology and linking these data to imaging and omics could develop a more accurate understanding of its role in symptomatic atherosclerosis.

The study design of AtherOMICS has several strengths. First, it integrates multiple omics modalities from plaque tissue and peripheral blood with noninvasive imaging, clinical data, and genotyping from the same study participants. This is reflected in our proteomic dataset of currently 88 plaque-plasma pairs with concurrent histology, imaging, and clinical information, allowing for the identification of circulating biomarkers that associate with specific plaque vulnerability features and different clinical presentations. Second, AtherOMICS collects plaque imaging from multiple modalities both in vivo (CTA and MRI from routine diagnostics and dedicated in vivo MRI substudy) and ex vivo (plaque tissue MRI). This approach enables imaging characterization of plaque vulnerability features through coregistration with histology. Third, plaque and blood

samples are collected and processed with long-term storage in mind. Different omics analyses can be executed on stored samples independently of each other and of the collection step, which enhances scalability and flexibility. Fourth, our annotation strategy for histology sections allows for a detailed atlas of plaque vulnerability features that carries information about number, shape, and spatial relationships of substructures, which will facilitate future efforts toward spatial omics. We believe that these aspects contribute to the utility of this resource.

AtherOMICS has specific limitations. First, patients undergoing endarterectomy typically exhibit advanced stages of atherosclerotic disease, which is reflected in an overrepresentation of type VI plaques and thus limits the interpretability of findings for less advanced atherosclerosis stages. Second, unlike, e.g., AtheroExpress, it does not follow up on patients after endarterectomy surgery, meaning that recurrent cardiovascular and cerebrovascular events are not captured. Third, several omics analyses, typically requiring very large sample sizes, are still underpowered. Other studies investigating proteomic changes in patients undergoing carotid endarterectomy leveraged cohorts of more than 500 participants (*61*, *62*). The pace of inclusion into AtherOMICS, which has stabilized around 88 to 92 participants per year (fig. S1A), suggests that at least 610 participants will be included by 2030 and 1050 by 2035. Nevertheless, an expansion of study inclusion to other centers would greatly increase the participant cohort and improve study power. Fourth, compared to the biobanking and clinical data components of the study, fewer patients agree to participate in the in vivo MRI substudy, thus limiting the pace of inclusion. Fifth, subclinical atherosclerosis or silent ischemic events in other vascular territories such as the coronary arteries could affect circulating biomarker profiles. Since 46% of asymptomatic patients reported a history of diagnosed coronary artery disease, silent ischemic events could influence our study findings. Sixth, AtherOMICS is currently limited to plaque tissue from the carotid and femoral arteries, which may affect the translation of findings to other vascular territories such as coronary or intracranial arteries (*63*). Seventh, although carotid ultrasound images and derived measurements such as intima-media thickness could be extracted from the medical records of currently 132 participants, this widely available and cost-effective imaging technique is currently not being used for investigations. Eighth, CTA data used in the study are obtained from clinical routine, which results in variable image quality depending on scanner type and scan parameters and affects concordance with study-specific imaging modalities and histology. Ninth, the monocentric study design results in an overrepresentation of urban-dwelling individuals of European ancestry.

In conclusion, AtherOMICS integrates deep multiomic profiling of human atherosclerotic plaques with conventional histopathology, clinical phenotyping, blood biobanking, and in vivo plaque imaging. This study protocol with initial pilot results is intended to increase the transparency and reproducibility of our study design, demonstrate feasibility ahead of downstream analyses, offer an outlook toward future research efforts, and invite collaboration. AtherOMICS has the potential to contribute novel insights into mechanisms underlying human atheroprogression, reveal the molecular signatures of plaque vulnerability, and develop noninvasive biomarkers of plaque instability.

MATERIALS AND METHODS

Detailed standard operating procedures underlying AtherOMICS can be found in the Supplementary Materials.

Study overview

The reporting of pilot data follows the STROBE guidelines for cross-sectional studies (*64*). AtherOMICS has been approved by the Ethics Committee of the Faculty of Medicine of the Ludwig-Maximilians-Universität (LMU) in Munich, Germany (approval numbers: 121-09, 22-0135, and 23-0772). All participants have provided written informed consent and the study conforms to the 2008 Declaration of Helsinki.

Recruitment for AtherOMICS began in August 2022 and includes the following (Fig. 1):

1) Plaque biobanking: Plaque material removed during carotid or femoral endarterectomy is collected and processed for histology, ex vivo MRI, and omics analyses.
2) Blood biobanking: Peripheral blood is collected from eligible participants before undergoing endarterectomy.
3) Clinical data collection: Demographic and anthropometric data, medical and medication history, and clinical laboratory data are collected from participants' medical records (table S4). In addition, a cardiovascular risk factor interview is conducted with participants by study personnel (table S5).
4) In vivo imaging: CTAs and brain MRIs are obtained from clinical routine diagnostics. A high-resolution carotid MRI scan is conducted with participants before surgery and independent from clinical imaging data collection.

Study participants

The target population of AtherOMICS includes adults scheduled to undergo carotid or femoral endarterectomy due to atherosclerotic disease. Participants are consecutively recruited from the Vascular Surgery and Neurology Departments at LMU Klinikum in Munich, Germany. Reasons for referral are symptomatic or asymptomatic carotid artery stenosis and symptomatic peripheral artery disease due to stenotic lesions in the femoral artery. Study team members identify potentially eligible participants by daily screening of hospital admission records and surgery plans. The inclusion criteria for the biobank are as follows:

1) Adults (age $\geq$ 18 years)
2) Scheduled for carotid or femoral endarterectomy in the next 7 days
3) Provision of written informed consent for the study before participation.

The exclusion criteria are as follows:

1) Inability or unwillingness to provide written informed consent
2) Prior ipsilateral endarterectomy or stenting
3) Prior local radiation therapy.

Consenting participants scheduled for carotid endarterectomy are additionally invited to participate in in vivo imaging assessment with carotid MRI before surgery. Team members performing eligibility screening are bound to uphold data protection requirements. A physician trained in Good Clinical Practice oversees screening activity and ultimately determines eligibility.

Once a patient's eligibility is confirmed during screening, they are contacted in person by a member of the study team, who explains the nature of the study using the study consent forms. Patients are then informed about their rights as participants in a clinical study. If patients express interest in participating and

once all questions have been addressed, then they are asked to sign the consent forms. Copies are provided for the participants' own records. Consent forms signed and dated by both parties are later stored at the research institution under restricted access. Once written informed consent is obtained, the team member conducts a structured interview for cardiovascular risk factors (table S5).

Plaque biobanking

Plaque material is collected directly from the operational room during endarterectomy immediately after plaque excision. Samples are transported to the processing facility on ice and in a falcon tube filled with sterile phosphate-buffered saline. The time between removal of plaque material from the affected artery to placement on ice is recorded. A randomly generated pseudonym is assigned to the sample for later reference. For processing, the plaque is photographed and then sectioned as follows (fig. S2): First, a 5-mm section containing the most diseased segment (MDS) in the internal carotid artery and a 5-mm marginal sections proximal and distal to the MDS are identified by morphological assessment and documented on the plaque outline. Then, the plaque is cut into the respective sections using scissors or a scalpel. The MDS is transferred to a tube and submerged in 4% paraformaldehyde (PFA) solution to be used for ex vivo MRI and histopathological analysis. Twenty-four hours after initiating PFA fixation, the MDS is removed and washed for 1 hour under lukewarm running water. Thereafter, the plaque is kept in 70% ethanol in an Eppendorf tube to undergo ex vivo MRI. Then, the plaque is decalcified at 4°C using a tris-buffered 200 mM EDTA solution at a pH of 8.0. Daily checks are performed where the section is morphologically assessed for successful decalcification, after which the plaque is transferred to temporary storage in a 70% ethanol solution. The remaining plaque segments are flash frozen by submersion in liquid nitrogen–cooled 2-methyl butane and stored at −80°C for subsequent omics analyses. The time between placement on ice in the operating room and flash-freezing is again recorded. Per protocol, the sum of table-to-ice-time and ice-to-flash time should not exceed 60 min to minimize RNA and protein degradation.

Histological processing

After dehydration and embedding in paraffin, MDS segments are sent out for histological processing at the Core Facility Pathology & Tissue Analytics, Helmholtz Munich, Germany. There, serial sections of 5 μm in thickness are taken from the MDS in 1-mm intervals. The sections undergo stainings with hematoxylin and eosin (H&E), anti–α–smooth muscle actin (αSMA) immunohistochemistry (IHC) for smooth muscle cells, anti-CD68 IHC for macrophages, and Picrosirius Red for collagen. IHC is performed using standard diaminobenzidine staining. Slides are scanned at high resolution with a microscope (Carl Zeiss NTS Ltd., Oberkochen, Germany). The resulting whole-slide images are stored in the .CZI format. For analysis, whole-slide images of up to three sections are automatically split into scenes containing one section each and imported into QuPath (v.0.4.4) (*65*). A set of unstained, unimaged slides is stored for future stainings.

IHC analysis

For cellular composition measurements (CD68 and αSMA), QuPath's segmentation feature is used to manually detect the positive region within the image that can be identified as objects in a hierarchical method below the annotations. These objects can be assigned defined colors in QuPath that classify DAB-stained area (immunostaining-positive, "brown"; immunostaining-negative) and background region devoid of tissue, based on the predictions at the region of interest at the same time. QuPath's random trees classifier feature consists of multiclass classification tasks that assign each pixel of the image to one of three categories, e.g., "positive," "negative," and "ignore" (no plaque region), which are used for model training. Thereby, values for immunostaining-positive area and remaining plaque area (both in square micrometers) are obtained (Fig. 1B). This workflow is implemented throughout the images of immunostained sections and resulting quantification data are collected in spreadsheets for later analysis. αSMA sections are quantified in moderate and CD68 samples in high resolution due to differences in color intensities.

Plaque feature annotation

Staff with experience in vascular histology and unaware of sample identity annotate plaque features using the geometry tools provided within the software. Sections are only annotated if they contain at least 50% of plaque circumference and are devoid of out-of-focus areas.

Total plaque area is determined through measuring the area of the entire plaque tissue captured in the H&E cross section and serves as a normalizing parameter for the other measurements. If large parts of the cross section are not represented in H&E but in other stainings at an adjacent level within 5 to 10 μm, then the other staining is used to impute total plaque area.

Lipid cores are detected and characterized in Sirius Red stainings (Fig. 1D). Their main distinguishing features are clefts resulting from dissolved cholesterol crystals, dark yellow (lipid-rich) matrix, the absence of collagen fibers in later lesional stages, and outlines of cellular debris throughout the core (*66*–*68*). As the unstable core tissue is often affected during processing, especially in ruptured plaques, parts of the lipid core are at times not accounted for in Sirius Red sections. In these cases, if the plaque geometry is unaffected and the surrounding plaque tissue permits the inference of original shape and size, then the lipid core area is reconstructed using directly adjacent sections and ex vivo MRI to confirm.

Calcification can be observed in H&E stainings (Fig. 1E). Despite the plaque tissue undergoing decalcification, the borders of previously fully calcified islets can usually be clearly delineated and inferred using matched ex vivo MRI, which is performed before decalcification. Sheet-calcified areas and calcified nodules exhibit a dark-purple to deep-blue staining in H&E, whereas microcalcifications display blue granular deposits within the extracellular matrix that is best contrasted from the surrounding, uncalcified tissue at larger magnification levels (*66*, *69*).

Neovascularization is determined by annotating each visible neovessel in any given H&E section (Fig. 1F). Neovessels are distinguished from other, irrelevant structures through judging the shape (mostly round, oval, or elongated), observing elongated endothelial cells surrounding the lumen, and the presence of red blood cells inside the lumen (*70*, *71*). The shape of the lumen is overlain with a geometric annotation to capture both total number and total area of neovessels per section.

IPH is typically detected in H&E and definitively identified using corroborating signatures in Sirius Red and CD68 stainings (Fig. 1G). IPHs present as either fresh, with large quantities of clearly delineable red blood cells present within plaque tissue with strong CD68-positive signal, or old IPH, with sparse or degraded-appearing red blood cells, clear borders between the light-pink–colored hemorrhage area and surrounding plaque tissue and a homogenous

structure that obscures the underlying plaque matrix (*71*, *72*). Occasionally, mixed forms can be observed that result from rehemorrhaging at the site of a previous IPH (*66*).

Plaque progression assessment (AHA classification grading)

Staff with experience in vascular histology and unaware of sample identity review H&E and Sirius Red stainings at the whole-section level and independently complete a standardized assessment based on the 1995 AHA classification (fig. S3) (*40*). Divergent assessments are noted and resolved by consensus.

Ex vivo MRI

MRI scanning is undertaken in a 3-T small animal scanner (nanoScan PET/MRI, Mediso, Münster, Germany) using a 30-mm-diameter birdcage coil within 1 to 4 days after excising specimen. Sequences were based on previously published data with minor changes (*73*). Quantitative T1/T2/T2* mapping sequences (qT1, qT2, and qT2*) and multicontrast fast spin echo (FSE) sequences including T1, T2, T2*, and proton density (PD)–weighted images are acquired in axial orientation. A multi-inversion recovery FSE sequence with 12 inversion times (30, 50, 80, 100, 300, 400, 500, 700, 800, 1000, 1200, and 1300 ms) is used for T1 mapping; a multiecho spin echo sequence with 14 echoes ranging from 10 to 140 ms with 10-ms steps is used for T2 mapping; and an interleaved multiecho GRE sequence with eight echoes ranging from 2.19 to 17.59 ms with 2.2-ms steps is used for T2* mapping. Scanning parameters are summarized in table S6. The PD values of plaque components are also quantified by normalizing the signal intensities on PD-weighted images, with the signal intensities of the healthy wall set to 1 as a reference.

Blood biobanking

Peripheral blood is collected in two 9-ml EDTA-coated tubes and one 7.5-ml serum tube (S-Monovette, Sarstedt, Nümbrecht, Germany). The serum and one EDTA tube are maintained in an upright position for 30 min at room temperature and then centrifuged at 2000*g* for 10 min at 15°C to separate serum and plasma. Aliquots of 8 × 300 μl for each serum and plasma are created in barcoded tubes, loaded onto 8 × 12 racks, and scanned into an internal database. The samples are stored at −80°C to be later used for omics analyses. The second EDTA-coated plasma tube is stored at 4°C for DNA extraction.

DNA extraction

DNA is extracted from participant plasma using commercially available NucleoSpin Blood XL tube and reagent kits (Macherey-Nagel, Düren, Germany), as well as the supplied protocol. Briefly, 250 μl of Proteinase K suspension (20 μg/ml) are added to 5 ml of EDTA plasma and incubated for 15 min at 56°C after adding the supplied buffer and vortexing the solution. When cooled to room temperature, 100% ethanol is added, and the entire solution is loaded onto the supplied filter columns. After centrifuging twice at 4000*g* for 3 min and removing the flow-through at both iterations, the remaining sample is washed twice under centrifugation using the supplied wash buffer. Elution is performed using 500 μl of 70°C warm BE buffer and incubated for 3 min and then centrifuged for another 2 min at 4000*g*. The eluate is then collected, and DNA concentration is measured using a NanoDrop 2000 spectrophotometer (Thermo Fisher Scientific, Waltham, MA, USA). Samples are then cataloged in an internal DNA database and stored at −80°C for later use.

Demographic and clinical data collection

Sociodemographic and anthropomorphic data are acquired from hospital records. Cardiovascular risk factors are assessed through a structured interview (table S5). Patients undergoing carotid endarterectomy are considered to be symptomatic if they report sudden-onset focal neurological symptoms consistent with cerebrovascular events ipsilateral to the stenosed carotid artery within the past 6 months or if these events are found in the patient records (*74*, *75*). A NASCET value obtained during clinical routine is extracted from past radiological or ultrasound examinations. "Cardiovascular medication" is defined as the current medications upon admission to the hospital that fall under one or more of the following categories: (i) antihypertensive, (ii) antidiabetic, (iii) lipid-modifying agent, (iv) antiplatelet agent or anticoagulant, and (v) diuretic. For clinical laboratory assessments, most recent values from the moment of surgery are extracted. It is not uncommon for the individual assessments (table S4) to be performed at different time points; therefore, the most recent leukocyte count and complement-reactive protein (CRP) measurements are extracted if they occurred up to 14 days before surgery. Total cholesterol, high-density lipoprotein (HDL), and low-density lipoprotein (LDL) measurements are extracted if they occurred up to 28 days before surgery.

In vivo imaging

We collect vascular and brain imaging studies from the medical records of the study participants. Specifically, we export pseudonymized imaging stacks in DICOM format from the most recent presurgery carotid CTA, brain, and cervical MRI, provided that this imaging has been conducted. The scans are acquired during routine clinical assessment, and scanner brand and parameter settings vary across patients.

Eligible participants are additionally invited to a presurgery high-resolution MRI of the carotid arteries and brain in the context of an imaging study nested within AtherOMICS. This scan is conducted specifically for the study and irrespectively of previous scans in the clinical context. A physician assesses whether contraindications for MRI are present and obtains separate written, informed consent from the participant. Participants unwilling or unable to undergo MRI can still participate in the biobank through collection of plaque material, blood samples, and clinical data.

CTA annotation strategy

CTA imaging stacks are exported from the clinical documentation system and loaded into 3DSlicer (v. 5.6.2) (*76*) for further processing. For total plaque, soft plaque, and calcification thickness measurements, the slice showing the maximum extent of the corresponding plaque component across the entire plaque was selected. Calcification location is similarly measured at the level with the maximum calcification burden and expressed as the relative luminal distance of the center of the largest calcification islet. This relative distance is determined by dividing the distance of the calcification islet from the lumen and the distance from the lumen to the outer vessel outline (*77*). The remodeling index was calculated as the ratio of the cross-sectional lumen area at the most stenotic site to the lumen area of the proximal reference (*78*). To obtain total calcification volume, calcified areas were manually delineated throughout the entire plaque. Mean calcification density was defined as the average Hounsfield unit value throughout the entire calcified volume (*79*).

In vivo MRI substudy

MRI scans are performed on a 3-T device (Magnetom Prisma, Siemens Healthineers, Erlangen, Germany) using a routine 32-channel head coil and two four-channel, special purpose carotid coils. The imaging protocol has been previously described (*80*, *81*). Briefly, it includes

time-of-flight (TOF) magnetic resonance angiography and black-blood T1-, PD-, and T2-weighted sequences with fat suppression. Study pseudonym, sex, and age are recorded, and imaging stacks are archived on a dedicated clinical imaging server inside the research facility.

We aim to pursue the integration of contrast-enhanced T1-weighted sequences. Patients without known intolerance to gadolinium and no evidence of severely impaired renal function (GFR ≤ 30 ml/min per kilogram) will also be administered gadolinium–diethylenetriamine pentaacetic acid–BMA (Gadobutrol, Bayer-Schering, Leverkusen, Germany) at a dosage of 0.1 ml/kg and at a rate of 3 ml/s, 5 min before postcontrast T1-weighted imaging.

Omics profiling

Single-nucleus RNA sequencing

Frozen plaque sections of 150 to 500 mg for 32 plaques were sent to Singleron Biotechnologies (Cologne, Germany) to perform snRNA-seq. Briefly, for library preparation, after tissue dissociation and cell lysis, nuclei were extracted, counted, and then adjusted to a concentration of 1×10^6/ml. Nuclei were suspended in a mixture with reverse transcriptase reagent containing template oligoprimers and reverse transcriptase. The solution was loaded onto a chip (SCOPE-chip) and surrounded by oil surfactant. Nuclei then form droplets with a bead gel containing unique molecular identifiers (UMIs) using a microfluidic double–cross-connection isolation system. Formed droplets were collected, cDNA fragments were reverse transcribed, and gel beads were subsequently dissolved, releasing the UMI-tagged amplification products. Barcoded fragments were pooled for library construction and then sequenced aiming for 6000 nuclei and 35,000 to 50,000 reads. Quality control was performed by examining tissue, nuclei, cDNA, and library yield and fragmentation. Nuclei from a total of 17 plaques passed quality control and were successfully sequenced.

Nuclei were retained using standard quality control thresholds (>150 detected genes, >150 UMIs, and <20% mitochondrial transcripts). Doublets were identified and removed on a per-sample basis using DoubletFinder, assuming an expected doublet rate of ~4% per library (*82*, *83*). Gene expression was normalized and variance stabilized using SCTransform, with mitochondrial content regressed out. Highly variable features ($n = 1500$) were selected across samples, and integration anchors were identified using FindIntegrationAnchors to generate a shared integrated assay via IntegrateData (*84*). Principal components analysis was performed on the integrated assay, and the first 15 components were used to construct a shared nearest-neighbor graph ($k = 40$). Clustering was performed using the Louvain algorithm with a resolution of 1.4. Broad lineage identities were assigned using canonical marker genes from published human vascular and atherosclerotic plaque single-cell atlases, together with the Human Cell Atlas as reference (*16*, *85*–*87*). Cluster-level profiles were evaluated using marker-based scoring, reference-based correlation (clustifyr), and gene set enrichment (GSVA/ssGSEA). Final annotations were defined on the basis of concordance across methods and manual inspection of marker expression.

Proteomics

We performed proteomic characterization of 88 matched plaque-plasma pairs. To guarantee sample integrity, both blood and plaque samples destined for proteomics analysis were stored at −80°C as described above. Radioimmunoprecipitation assay lysis buffer with added cOmplete mini protease inhibitor cocktail (Sigma-Aldrich, St. Louis, MI, USA) was used for cell lysis. Plaque samples were thawed on ice, homogenized in the lysis buffer, and centrifuged to remove debris. The resulting supernatant was stored at −80°C until further use. Plaque lysates were subjected to SDS–polyacrylamide gel electrophoresis and subsequent Coomassie Blue staining, whereafter gels were inspected visually for signs of protein degradation. Pseudonymized plaque lysates and plasma aliquots were shipped on dry ice to Helmholtz Munich, Germany on 96-well polymerase chain reaction plates specified by the assay provider. Proteomic profiling was performed using Olink Explore 3072 panel, a proximity extension assay platform that uses DNA-conjugated antibodies and subsequent DNA amplification and sequencing to determine protein abundance (*88*). The resulting C_t values were converted into normalized protein expression (NPX), a surrogate marker of protein concentration, through adjusting for interplate correction factors. Last, mean NPX values from a total of 2841 proteins in both plaque and plasma were compared between symptomatic and asymptomatic patients. In addition, associations between plaque and plasma NPX values for any given protein were examined through calculating Spearman's rank correlation coefficients.

Supplementary Materials

This PDF file includes:

Figs. S1 to S4
Tables S1 to S6
Standard Operating Procedures

REFERENCES

1. GBD 2023 Causes of Death Collaborators, Global burden of 292 causes of death in 204 countries and territories and 660 subnational locations, 1990–2023: A systematic analysis for the Global Burden of Disease Study 2023. *Lancet* **406**, 1811–1872 (2025).
2. C. A. Gleissner, Translational atherosclerosis research: From experimental models to coronary artery disease in humans. *Atherosclerosis* **248**, 110–116 (2016).
3. P. Libby, The changing landscape of atherosclerosis. *Nature* **592**, 524–533 (2021).
4. P. M. Ridker, J. G. MacFadyen, B. M. Everett, P. Libby, T. Thuren, R. J. Glynn, Cantos Trial Group, Relationship of C-reactive protein reduction to cardiovascular event reduction following treatment with canakinumab: A secondary analysis from the CANTOS randomised controlled trial. *Lancet* **391**, 319–328 (2018).
5. J.-C. Tardif, S. Kouz, D. D. Waters, O. F. Bertrand, R. Diaz, A. P. Maggioni, F. J. Pinto, R. Ibrahim, H. Gamra, G. S. Kiwan, C. Berry, J. López-Sendón, P. Ostadal, W. Koenig, D. Angoulvant, J. C. Grégoire, M.-A. Lavoie, M.-P. Dubé, D. Rhainds, M. Provencher, L. Blondeau, A. Orfanos, P. L. L'Allier, M.-C. Guertin, F. Roubille, Efficacy and safety of low-dose colchicine after myocardial infarction. *N. Engl. J. Med.* **381**, 2497–2505 (2019).
6. S. M. Nidorf, A. T. L. Fiolet, A. Mosterd, J. W. Eikelboom, A. Schut, T. S. J. Opstal, S. H. K. The, X.-F. Xu, M. A. Ireland, T. Lenderink, D. Latchem, P. Hoogslag, A. Jerzewski, P. Nierop, A. Whelan, R. Hendriks, H. Swart, J. Schaap, A. F. M. Kuijper, M. W. J. van Hessen, P. Saklani, I. Tan, A. G. Thompson, A. Morton, C. Judkins, W. A. Bax, M. Dirksen, M. Alings, G. J. Hankey, C. A. Budgeon, J. G. P. Tijssen, J. H. Cornel, P. L. Thompson, Colchicine in patients with chronic coronary disease. *N. Engl. J. Med.* **383**, 1838–1847 (2020).
7. J. Fan, T. Watanabe, Atherosclerosis: Known and unknown. *Pathol. Int.* **72**, 151–160 (2022).
8. P. Libby, J. E. Buring, L. Badimon, G. K. Hansson, J. Deanfield, M. S. Bittencourt, L. Tokgözoğlu, E. F. Lewis, P. Libby, J. E. Buring, L. Badimon, G. K. Hansson, J. Deanfield, M. S. Bittencourt, L. Tokgözoğlu, E. F. Lewis, Atherosclerosis. *Nat. Rev. Dis. Primers* **5**, 56 (2019).
9. L. T. May, B. A. Bartolo, D. G. Harrison, T. Guzik, G. R. Drummond, G. A. Figtree, R. H. Ritchie, K.-A. Rye, J. B. de Haan, Translating atherosclerosis research from bench to bedside: Navigating the barriers for effective preclinical drug discovery. *Clin. Sci.* **136**, 1731–1758 (2022).
10. G. Pasterkamp, H. M. den Ruijter, C. Giannarelli, False Utopia of one unifying description of the vulnerable atherosclerotic plaque: A call for recalibration that appreciates the diversity of mechanisms leading to atherosclerotic disease. *Arterioscler. Thromb. Vasc. Biol.* **42**, e86–e95 (2022).
11. R. A. van Dijk, R. Kleemann, A. F. Schaapherder, A. van den Bogaerdt, U. Hedin, L. Matic, J. H. N. Lindeman, Validating human and mouse tissues commonly used in atherosclerosis research with coronary and aortic reference tissue: Similarities but

profound differences in disease initiation and plaque stability. *JVS Vasc. Sci.* **4**, 100118 (2023).
12. R. Ross, J. Glomset, L. Harker, Response to injury and atherogenesis. *Am. J. Pathol.* **86**, 675–684 (1977).
13. M. B. Furie, R. N. Mitchell, Plaque attack: One hundred years of atherosclerosis in the american journal of pathology. *Am. J. Pathol.* **180**, 2184–2187 (2012).
14. J. Tan, Y. Liang, Z. Yang, Q. He, J. Tong, Y. Deng, W. Guo, K. Liang, J. Tang, W. Shi, B. Yu, Single-cell transcriptomics reveals crucial cell subsets and functional heterogeneity associated with carotid atherosclerosis and cerebrovascular events. *Arterioscler. Thromb. Vasc. Biol.* **43**, 2312–2332 (2023).
15. M. Mokry, A. Boltjes, L. Slenders, G. Bel-Bordes, K. Cui, E. Brouwer, J. M. Mekke, M. A. C. Depuydt, N. Timmerman, F. Waissi, M. C. Verwer, A. W. Turner, M. D. Khan, C. J. Hodonsky, E. Diez Benavente, R. J. G. Hartman, N. A. M. van den Dungen, N. Lansu, E. Nagyova, K. H. M. Prange, J. C. Kovacic, J. L. M. Björkegren, E. Pavlos, E. Andreakos, H. Schunkert, G. K. Owens, C. Monaco, A. V. Finn, R. Virmani, N. J. Leeper, M. P. J. de Winther, J. Kuiper, G. J. de Borst, E. S. G. Stroes, M. Civelek, D. P. V. de Kleijn, H. M. den Ruijter, F. W. Asselbergs, S. W. van der Laan, C. L. Miller, G. Pasterkamp, Transcriptomic-based clustering of human atherosclerotic plaques identifies subgroups with different underlying biology and clinical presentation. *Nat. Cardiovasc. Res.* **1**, 1140–1155 (2022).
16. M. A. C. Depuydt, K. H. M. Prange, L. Slenders, T. Ord, D. Elbersen, A. Boltjes, S. C. A. de Jager, F. W. Asselbergs, G. J. de Borst, E. Aavik, T. Lonnberg, E. Lutgens, C. K. Glass, H. M. den Ruijter, M. U. Kaikkonen, I. Bot, B. Slutter, S. W. van der Laan, S. Yla-Herttuala, M. Mokry, J. Kuiper, M. P. J. de Winther, G. Pasterkamp, Microanatomy of the human atherosclerotic plaque by single-cell transcriptomics. *Circ. Res.* **127**, 1437–1455 (2020).
17. K. Palm, K. Theofilatos, S. Van Der Laan, E. D. Benavente, G. De Borst, D. De Kleijn, J. Wotja, M. Mayr, H. Den Ruijter, M. Mokry, G. Pasterkamp, Proteomic profiling reveals higher presence of glycolytic enzymes in vulnerable atherosclerotic lesions. *Atherosclerosis* **395**, 117698 (2024).
18. X. Wu, H. Zhang, Omics approaches unveiling the biology of human atherosclerotic plaques. *Am. J. Pathol.* **194**, 482–498 (2024).
19. N. S. Nurmohamed, J. M. Kraaijenhof, M. Mayr, S. J. Nicholls, W. Koenig, A. L. Catapano, E. S. G. Stroes, Proteomics and lipidomics in atherosclerotic cardiovascular disease risk prediction. *Eur. Heart J.* **44**, 1594–1607 (2023).
20. F. Barkas, Y. Z. Sener, P. A. Golforoush, A. Kheirkhah, E. Rodriguez-Sanchez, J. Novak, M. Apellaniz-Ruiz, R. K. Akyea, V. Bianconi, A. Ceasovschih, Y. J. Chee, M. Cherska, J. R. Chora, M. D'Oria, N. Demikhova, D. Kocyigit Burunkaya, A. Rimbert, C. Macchi, K. Rathod, L. Roth, V. Sukhorukov, S. Stoica, R. Scicali, T. Storozhenko, J. Uzokov, M. G. Lupo, E. P. C. van der Vorst, F. Porsch, Advancements in risk stratification and management strategies in primary cardiovascular prevention. *Atherosclerosis* **395**, 117579 (2024).
21. P. Brindle, A. Beswick, T. Fahey, S. Ebrahim, Accuracy and impact of risk assessment in the primary prevention of cardiovascular disease: A systematic review. *Heart* **92**, 1752–1759 (2006).
22. L. Saba, M. Anzidei, B. C. Marincola, M. Piga, E. Raz, P. P. Bassareo, A. Napoli, L. Mannelli, C. Catalano, M. Wintermark, L. Saba, M. Anzidei, B. C. Marincola, M. Piga, E. Raz, P. P. Bassareo, A. Napoli, L. Mannelli, C. Catalano, M. Wintermark, Imaging of the carotid artery vulnerable plaque. *Cardiovasc. Radiol.* **37**, 572–585 (2014).
23. Z. Mei, L. Xu, Q. Huang, C. Lin, M. Yu, S. Shali, H. Wu, Y. Lu, R. Wu, Z. Wang, L. Luo, Z. Sun, L. Sun, J. Qian, G. Chen, H. Tang, K. Yao, Y. Zheng, Y. Dai, J. Ge, Metabonomic biomarkers of plaque burden and instability in patients with coronary atherosclerotic disease after moderate lipid-lowering therapy. *J. Am. Heart Assoc.* **13**, e036906 (2024).
24. W. Koenig, High-sensitivity C-reactive protein and atherosclerotic disease: From improved risk prediction to risk-guided therapy. *Int. J. Cardiol.* **168**, 5126–5134 (2013).
25. S. Liang, J. Willis, J. Dou, V. Mohanty, Y. Huang, E. Vilar, K. Chen, Sensei: How many samples to tell a change in cell type abundance? *BMC Bioinformatics* **23**, 2 (2022).
26. G. Izmirlian, Strong consistency and asymptotic normality for quantities related to the Benjamini–Hochberg false discovery rate procedure. *Stat. Probab. Lett.* **160**, 108713 (2020).
27. G. Izmirlian, L. A. Sirota, V. W. Berger, V. Kipnis, The fundamentals of multiplicity adjustment in biostatistics. *J. Natl. Cancer Inst. Monogr.* **2025**, 10–13 (2025).
28. P. de Valpine, H.-M. Bitter, M. P. S. Brown, J. Heller, A simulation-approximation approach to sample size planning for high-dimensional classification studies. *Biostatistics* **10**, 424–435 (2009).
29. R. J. Lusby, L. D. Ferrell, W. K. Ehrenfeld, R. J. Stoney, E. J. Wylie, Carotid plaque hemorrhage. Its role in production of cerebral ischemia: Its role in production of cerebral ischemia. *Arch. Surg.* **117**, 1479–1488 (1982).
30. A. C. Bashore, H. Yan, C. Xue, L. Y. Zhu, E. Kim, T. Mawson, J. Coronel, A. Chung, N. Sachs, S. Ho, L. S. Ross, M. Kissner, E. Passegue, R. C. Bauer, L. Maegdefessel, M. Li, M. P. Reilly, High-dimensional single-cell multimodal landscape of human carotid atherosclerosis. *Arterioscler. Thromb. Vasc. Biol.* **44**, 930–945 (2024).
31. A. Papadopoulos, K. Palaiopanos, H. Björkbacka, A. Peters, J. A. de Lemos, S. Seshadri, M. Dichgans, M. K. Georgakis, Circulating interleukin-6 levels and incident ischemic stroke. *Neurology* **98**, e1002–e1012 (2022).
32. K. G. Aragam, T. Jiang, A. Goel, S. Kanoni, B. N. Wolford, D. S. Atri, E. M. Weeks, M. Wang, G. Hindy, W. Zhou, C. Grace, C. Roselli, N. A. Marston, F. K. Kamanu, I. Surakka, L. M. Venegas, P. Sherliker, S. Koyama, K. Ishigaki, B. O. Åsvold, M. R. Brown, B. Brumpton, P. S. de Vries, O. Giannakopoulou, P. Giardoglou, D. F. Gudbjartsson, U. Güldener, S. M. I. Haider, A. Helgadottir, M. Ibrahim, A. Kastrati, T. Kessler, T. Kyriakou, T. Konopka, L. Li, L. Ma, T. Meitinger, S. Mucha, M. Munz, F. Murgia, J. B. Nielsen, M. M. Nöthen, S. Pang, T. Reinberger, G. Schnitzler, D. Smedley, G. Thorleifsson, M. von Scheidt, J. C. Ulirsch, D. O. Arnar, N. P. Burtt, M. C. Costanzo, J. Flannick, K. Ito, D.-K. Jang, Y. Kamatani, A. V. Khera, I. Komuro, I. J. Kullo, L. A. Lotta, C. P. Nelson, R. Roberts, G. Thorgeirsson, U. Thorsteinsdottir, T. R. Webb, A. Baras, J. L. M. Björkegren, E. Boerwinkle, G. Dedoussis, H. Holm, K. Hveem, O. Melander, A. C. Morrison, M. Orho-Melander, L. S. Rallidis, A. Ruusalepp, M. S. Sabatine, K. Stefansson, P. Zalloua, P. T. Ellinor, M. Farrall, J. Danesh, C. T. Ruff, H. K. Finucane, J. C. Hopewell, R. Clarke, R. M. Gupta, J. Erdmann, N. J. Samani, H. Schunkert, H. Watkins, C. J. Willer, P. Deloukas, S. Kathiresan, A. S. Butterworth, K. G. Aragam, T. Jiang, A. Goel, S. Kanoni, B. N. Wolford, D. S. Atri, E. M. Weeks, M. Wang, G. Hindy, W. Zhou, C. Grace, C. Roselli, N. A. Marston, F. K. Kamanu, I. Surakka, L. M. Venegas, P. Sherliker, S. Koyama, K. Ishigaki, B. O. Åsvold, M. R. Brown, B. Brumpton, P. S. de Vries, O. Giannakopoulou, P. Giardoglou, D. F. Gudbjartsson, U. Güldener, S. M. I. Haider, A. Helgadottir, M. Ibrahim, A. Kastrati, T. Kessler, T. Kyriakou, T. Konopka, L. Li, L. Ma, T. Meitinger, S. Mucha, M. Munz, F. Murgia, J. B. Nielsen, M. M. Nöthen, S. Pang, T. Reinberger, G. Schnitzler, D. Smedley, G. Thorleifsson, M. von Scheidt, J. C. Ulirsch, D. O. Arnar, N. P. Burtt, M. C. Costanzo, J. Flannick, K. Ito, D.-K. Jang, Y. Kamatani, A. V. Khera, I. Komuro, I. J. Kullo, L. A. Lotta, C. P. Nelson, R. Roberts, G. Thorgeirsson, U. Thorsteinsdottir, T. R. Webb, A. Baras, J. L. M. Björkegren, E. Boerwinkle, G. Dedoussis, H. Holm, K. Hveem, O. Melander, A. C. Morrison, M. Orho-Melander, L. S. Rallidis, A. Ruusalepp, M. S. Sabatine, K. Stefansson, P. Zalloua, P. T. Ellinor, M. Farrall, J. Danesh, C. T. Ruff, H. K. Finucane, J. C. Hopewell, R. Clarke, R. M. Gupta, J. Erdmann, N. J. Samani, H. Schunkert, H. Watkins, C. J. Willer, P. Deloukas, S. Kathiresan, A. S. Butterworth, Discovery and systematic characterization of risk variants and genes for coronary artery disease in over a million participants. *Nat. Genet.* **54**, 1803–1815 (2022).
33. A. Mishra, R. Malik, T. Hachiya, T. Jurgenson, S. Namba, D. C. Posner, F. K. Kamanu, M. Koido, Q. Le Grand, M. Shi, Y. He, M. K. Georgakis, I. Caro, K. Krebs, Y. C. Liaw, F. C. Vaura, K. Lin, B. S. Winsvold, V. Srinivasasainagendra, L. Parodi, H. J. Bae, G. Chauhan, M. R. Chong, L. Tomppo, R. Akinyemi, G. V. Roshchupkin, N. Habib, Y. H. Jee, J. Q. Thomassen, V. Abedi, J. Carcel-Marquez, M. Nygaard, H. L. Leonard, C. Yang, E. Yonova-Doing, M. J. Knol, A. J. Lewis, R. L. Judy, T. Ago, P. Amouyel, N. D. Armstrong, M. K. Bakker, T. M. Bartz, D. A. Bennett, J. C. Bis, C. Bordes, S. Borte, A. Cain, P. M. Ridker, K. Cho, Z. Chen, C. Cruchaga, J. W. Cole, P. L. de Jager, R. de Cid, M. Endres, L. E. Ferreira, M. I. Geerlings, N. C. Gasca, V. Gudnason, J. Hata, J. He, A. K. Heath, Y. L. Ho, A. S. Havulinna, J. C. Hopewell, H. I. Hyacinth, M. Inouye, M. A. Jacob, C. E. Jeon, C. Jern, M. Kamouchi, K. L. Keene, T. Kitazono, S. J. Kittner, T. Konuma, A. Kumar, P. Lacaze, L. J. Launer, K. J. Lee, K. Lepik, J. Li, L. Li, A. Manichaikul, H. S. Markus, N. A. Marston, T. Meitinger, B. D. Mitchell, F. A. Montellano, T. Morisaki, T. H. Mosley, M. A. Nalls, B. G. Nordestgaard, M. J. O'Donnell, Y. Okada, N. C. Onland-Moret, B. Ovbiagele, A. Peters, B. M. Psaty, S. S. Rich, J. Rosand, M. S. Sabatine, R. L. Sacco, D. Saleheen, E. C. Sandset, V. Salomaa, M. Sargurupremraj, M. Sasaki, C. L. Satizabal, C. O. Schmidt, A. Shimizu, N. L. Smith, K. L. Sloane, Y. Sutoh, Y. V. Sun, K. Tanno, S. Tiedt, T. Tatlisumak, N. P. Torres-Aguila, H. K. Tiwari, D. A. Tregouet, S. Trompet, A. M. Tuladhar, A. Tybjaerg-Hansen, M. van Vugt, R. Vibo, S. S. Verma, K. L. Wiggins, P. Wennberg, D. Woo, P. W. F. Wilson, H. Xu, Q. Yang, K. Yoon, The COMPASS Consortium, The INVENT Consortium, The Dutch Parelsnoer Initiative (PSI), Cerebrovascular Disease Study Group, The Estonian Biobank, The PRECISE4Q Consortium, The FinnGen Consortium, The NINDS Stroke Genetics Network (SiGN), The MEGASTROKE Consortium, The SIREN Consortium, The China Kadoorie Biobank Collaborative Group, The VA Million Veteran Program, The International Stroke Genetics Consortium (ISGC), The Biobank Japan, The CHARGE Consortium, The GIGASTROKE Consortium, I. Y. Millwood, C. Gieger, T. Ninomiya, H. J. Grabe, J. W. Jukema, I. L. Rissanen, D. Strbian, Y. J. Kim, P. H. Chen, E. Mayerhofer, J. M. M. Howson, M. R. Irvin, H. Adams, S. Wassertheil-Smoller, K. Christensen, M. A. Ikram, T. Rundek, B. B. Worrall, G. M. Lathrop, M. Riaz, E. M. Simonsick, J. Korv, P. H. C. Franca, R. Zand, K. Prasad, R. Frikke-Schmidt, F. E. de Leeuw, T. Liman, K. G. Haeusler, Y. M. Ruigrok, P. U. Heuschmann, W. T. Longstreth, K. J. Jung, L. Bastarache, G. Pare, S. M. Damrauer, D. I. Chasman, J. I. Rotter, C. D. Anderson, J. A. Zwart, T. J. Niiranen, M. Fornage, Y. P. Liaw, S. Seshadri, I. Fernandez-Cadenas, R. G. Walters, C. T. Ruff, M. O. Owolabi, J. E. Huffman, L. Milani, Y. Kamatani, M. Dichgans, S. Debette, Stroke genetics informs drug discovery and risk prediction across ancestries. *Nature* **611**, 115–123 (2022).
34. S. Koyama, X. Liu, Y. Koike, K. Hikino, M. Koido, W. Li, K. Akaki, K. Tomizuka, S. Ito, N. Otomo, H. Suetsugu, S. Yoshino, M. Akiyama, K. Saito, Y. Ishikawa, C. Benner, P. Natarajan, P. T. Ellinor, T. Mushiroda, M. Horikoshi, M. Ikeda, N. Iwata, K. Matsuda, Biobank Japan Project, S. Niida, K. Ozaki, Y. Momozawa, S. Ikegawa, O. Takeuchi, K. Ito,

C. Terao, Population-specific putative causal variants shape quantitative traits. *Nat. Genet.* **56**, 2027–2035 (2024).
35. E. Cano-Gamez, K. L. Burnham, C. Goh, A. Allcock, Z. H. Malick, L. Overend, A. Kwok, D. A. Smith, H. Peters-Sengers, D. Antcliffe, G. A. S. Investigators, S. McKechnie, B. P. Scicluna, T. van der Poll, A. C. Gordon, C. J. Hinds, E. E. Davenport, J. C. Knight, N. Webster, H. Galley, J. Taylor, S. Hall, J. Addison, S. Roughton, H. Tennant, A. Guleri, N. Waddington, D. Arawwawala, J. Durcan, A. Short, K. Swan, S. Williams, S. Smolen, C. Mitchell-Inwang, T. Gordon, E. Errington, M. Templeton, P. Venatesh, G. Ward, M. McCauley, S. Baudouin, C. Higham, J. Soar, S. Grier, E. Hall, S. Brett, D. Kitson, R. Wilson, L. Mountford, J. Moreno, P. Hall, J. Hewlett, S. McKechnie, C. Garrard, J. Millo, D. Young, P. Hutton, P. Parsons, A. Smiths, R. Faras-Arraya, J. Soar, P. Raymode, J. Thompson, S. Bowrey, S. Kazembe, N. Rich, P. Andreou, D. Hales, E. Roberts, S. Fletcher, M. Rosbergen, G. Glister, J. M. Cuesta, J. Bion, J. Millar, E. J. Perry, H. Willis, N. Mitchell, S. Ruel, R. Carrera, J. Wilde, A. Nilson, S. Lees, A. Kapila, N. Jacques, J. Atkinson, A. Brown, H. Prowse, A. Krige, M. Bland, L. Bullock, D. Harrison, G. Mills, J. Humphreys, K. Armitage, S. Laha, J. Baldwin, A. Walsh, N. Doherty, S. Drage, L. O.-R. de Gordoa, S. Lowes, C. Higham, H. Walsh, V. Calder, C. Swan, H. Payne, D. Higgins, S. Andrews, S. Mappleback, C. Hind, C. Garrard, D. Watson, E. McLees, A. Purdy, M. Stotz, A. Ochelli-Okpue, S. Bonner, I. Whitehead, K. Hugil, V. Goodridge, L. Cawthor, M. Kuper, S. Pahary, G. Bellingan, R. Marshall, H. Montgomery, J. H. Ryu, G. Bercades, S. Boluda, A. Bentley, K. Mccalman, F. Jefferies, J. Knight, E. Davenport, K. Burnham, N. Maugeri, J. Radhakrishnan, Y. Mi, A. Allcock, C. Goh, An immune dysfunction score for stratification of patients with acute infection based on whole-blood gene expression. *Sci. Transl. Med.* **14**, eabq4433 (2022).
36. C. J. Hodonsky, A. W. Turner, M. D. Khan, N. B. Barrientos, R. Methorst, L. Ma, N. G. Lopez, J. V. Mosquera, G. Auguste, E. Farber, W. F. Ma, D. Wong, S. Onengut-Gumuscu, M. Kavousi, P. A. Peyser, S. W. van der Laan, N. J. Leeper, J. C. Kovacic, J. L. M. Björkegren, C. L. Miller, Multi-ancestry genetic analysis of gene regulation in coronary arteries prioritizes disease risk loci. *Cell Genom.* **4**, 100465 (2024).
37. A. Ray, P. Alabarse, R. Malik, M. Sargurupremraj, J. Bernhagen, M. Dichgans, S.-E. Baumeister, M. K. Georgakis, Single-cell transcriptome-wide Mendelian randomization and colocalization analyses uncover cell-specific mechanisms in atherosclerotic cardiovascular disease. *Am. J. Hum. Genet.* **112**, 1597–1609 (2025).
38. E. V. Minikel, J. L. Painter, C. C. Dong, M. R. Nelson, Refining the impact of genetic evidence on clinical success. *Nature* **629**, 624–629 (2024).
39. M. R. Nelson, H. Tipney, J. L. Painter, J. Shen, P. Nicoletti, Y. Shen, A. Floratos, P. C. Sham, M. J. Li, J. Wang, L. R. Cardon, J. C. Whittaker, P. Sanseau, The support of human genetic evidence for approved drug indications. *Nat. Genet.* **47**, 856–860 (2015).
40. H. C. Stary, A. B. Chandler, R. E. Dinsmore, V. Fuster, S. Glagov, W. Insull, M. E. Rosenfeld, C. J. Schwartz, W. D. Wagner, R. W. Wissler, A definition of advanced types of atherosclerotic lesions and a histological classification of atherosclerosis. *Circulation* **92**, 1355–1374 (1995).
41. J.-B. Michel, J. L. Martin-Ventura, A. Nicoletti, B. Ho-Tin-Noé, Pathology of human plaque vulnerability: Mechanisms and consequences of intraplaque haemorrhages. *Atherosclerosis* **234**, 311–319 (2014).
42. J. Montaner, L. Ramiro, A. Simats, S. Tiedt, K. Makris, G. C. Jickling, S. Debette, J.-C. Sanchez, A. Bustamante, Multilevel omics for the discovery of biomarkers and therapeutic targets for stroke. *Nat. Rev. Neurol.* **16**, 247–264 (2020).
43. L. Saba, R. Cau, A. Murgia, A. N. Nicolaides, M. Wintermark, M. Castillo, D. Staub, S. K. Kakkos, Q. Yang, K. I. Paraskevas, C. Yuan, M. Edjlali, R. Sanfilippo, J. Hendrikse, E. Johansson, M. Mossa-Basha, N. Balu, M. Dichgans, D. Saloner, D. Bos, H. R. Jager, R. Naylor, G. Faa, J. S. Suri, J. Costello, D. P. Auer, J. S. McNally, L. H. Bonati, V. Nardi, A. van der Lugt, M. Griffin, B. A. Wasserman, M. E. Kooi, J. Gillard, G. Lanzino, D. P. Mikhailidis, D. M. Mandell, J. C. Benson, D. H. K. van Dam-Nolen, A. Kopczak, J. W. Song, A. Gupta, J. K. DeMarco, S. Chaturvedi, R. Virmani, T. S. Hatsukami, M. Brown, A. R. Moody, P. Libby, A. Schindler, T. Saam, Carotid plaque-RADS: A novel stroke risk classification system. *JACC Cardiovasc. Imaging* **17**, 62–75 (2024).
44. J.-B. Michel, R. Virmani, E. Arbustini, G. Pasterkamp, Intraplaque haemorrhages as the trigger of plaque vulnerability. *Eur. Heart J.* **32**, 1977–1985 (2011).
45. G. W. van Lammeren, G. Pasterkamp, J.-P. P. M. de Vries, L. Bosch, J. J. de Haan, D. P. V. de Kleijn, F. L. Moll, A. Vink, Platelets enter atherosclerotic plaque via intraplaque microvascular leakage and intraplaque hemorrhage: A histopathological study in carotid plaques. *Atherosclerosis* **222**, 355–359 (2012).
46. J. C. Sluimer, F. D. Kolodgie, A. P. J. J. Bijnens, K. Maxfield, E. Pacheco, B. Kutys, H. Duimel, P. M. Frederik, V. W. M. van Hinsbergh, R. Virmani, M. J. A. P. Daemen, Thin-walled microvessels in human coronary atherosclerotic plaques show incomplete endothelial junctions relevance of compromised structural integrity for intraplaque microvascular leakage. *J. Am. Coll. Cardiol.* **53**, 1517–1527 (2009).
47. T. Bleckwehl, A. Babler, M. Tebens, S. Maryam, M. Nyberg, M. Bosteen, M. Halder, I. Shaw, S. Fleig, C. Pyke, H. Hvid, L. M. Voetmann, J. D. van Buul, J. C. Sluimer, V. Das, S. Baumgart, R. Kramann, S. Hayat, Encompassing view of spatial and single-cell RNA sequencing renews the role of the microvasculature in human atherosclerosis. *Nat. Cardiovasc. Res.* **4**, 26–44 (2025).
48. J. Pauli, D. Garger, F. Peymani, J. Wettich, N. Sachs, J. Wirth, K. Steiger, H. Zhang, I. Tabas, A. Tall, M. Li, M. P. Reilly, D. Branzan, H. Prokisch, M. P. Menden, L. Maegdefessel, Single cell spatial transcriptomics integration deciphers the morphological heterogeneity of atherosclerotic carotid arteries. *Nat. Commun.* **16**, 11282 (2025).
49. S. Raju, M. E. Turner, C. Cao, M. Abdul-Samad, N. Punwasi, M. C. Blaser, R. M. E. Cahalane, S. R. Botts, K. Prajapati, S. Patel, R. Wu, D. Gustafson, N. J. Galant, L. Fiddes, M. Chemaly, U. Hedin, L. Matic, M. A. Seidman, V. Subasri, S. A. Singh, E. Aikawa, J. E. Fish, K. L. Howe, Multiomic landscape of extracellular vesicles in human carotid atherosclerotic plaque reveals endothelial communication networks. *Arterioscler. Thromb. Vasc. Biol.* **45**, 1277–1305 (2025).
50. L. P. Matic, M. Jesus Iglesias, M. Vesterlund, M. Lengquist, M.-G. Hong, S. Saieed, L. Sanchez-Rivera, M. Berg, A. Razuvaev, M. Kronqvist, K. Lund, K. Caidahl, P. Gillgren, F. Pontén, M. Uhlén, J. M. Schwenk, G. K. Hansson, G. Paulsson-Berne, E. Fagman, J. Roy, R. Hultgren, G. Bergström, J. Lehtiö, J. Odeberg, U. Hedin, Novel multiomics profiling of human carotid atherosclerotic plaques and plasma reveals biliverdin reductase B as a marker of intraplaque hemorrhage. *JACC Basic Transl. Sci.* **3**, 464–480 (2018).
51. L. Jonasson, J. Holm, O. Skalli, G. Bondjers, G. K. Hansson, Regional accumulations of T cells, macrophages, and smooth muscle cells in the human atherosclerotic plaque. *Arteriosclerosis* **6**, 131–138 (1986).
52. L. Dib, L. A. Koneva, A. Edsfeldt, Y.-X. Zurke, J. Sun, M. Nitulescu, M. Attar, E. Lutgens, S. Schmidt, M. W. Lindholm, R. P. Choudhury, I. Cassimjee, R. Lee, A. Handa, I. Goncalves, S. N. Sansom, C. Monaco, Lipid-associated macrophages transition to an inflammatory state in human atherosclerosis, increasing the risk of cerebrovascular complications. *Nat. Cardiovasc. Res.* **2**, 656–672 (2023).
53. K. H. M. Prange, G. Bel-Bordes, M. A. C. Depuydt, P. Barlampas, M. J. Reif, M. L. B. Grönloh, R. W. M. Kempkes, G. R. Griffith, C. van Roomen, Y. Zhu, A. Edsfeldt, J. Sun, M. J. M. de Jong, B. M. Mol, B. Slütter, I. Bot, A. E. Neele, D. P. V. de Kleijn, G. J. de Borst, J. Kroon, A. Wezel, H. J. Smeets, E. S. G. Stroes, J. D. van Buul, P. Goossens, J. Kuiper, I. Goncalves, G. Pasterkamp, M. Mokry, M. P. J. de Winther, Carotid plaque macrophage burden and inflammatory lipid-associated macrophage markers predict secondary major adverse cardiovascular events after endarterectomy. *Eur. Heart J.* **47**, 3821–3836 (2026).
54. J. W. Williams, H. Winkels, C. P. Durant, K. Zaitsev, Y. Ghosheh, K. Ley, Single cell RNA sequencing in atherosclerosis research. *Circ. Res.* **126**, 1112–1126 (2020).
55. T. T. de Weert, H. Cakir, S. Rozie, S. Cretier, E. Meijering, D. W. J. Dippel, A. van der Lugt, Intracranial internal carotid artery calcifications: Association with vascular risk factors and ischemic cerebrovascular disease. *AJNR Am. J. Neuroradiol.* **30**, 177–184 (2009).
56. B. Verhoeven, W. E. Hellings, F. L. Moll, J. P. de Vries, D. P. V. de Kleijn, P. de Bruin, E. Busser, A. H. Schoneveld, G. Pasterkamp, Carotid atherosclerotic plaques in patients with transient ischemic attacks and stroke have unstable characteristics compared with plaques in asymptomatic and amaurosis fugax patients. *J. Vasc. Surg.* **42**, 1075–1081 (2005).
57. L. Saba, V. Nardi, R. Cau, A. Gupta, H. Kamel, J. S. Suri, A. Balestrieri, T. Congiu, A. P. H. Butler, S. Gieseg, D. Fanni, G. Cerrone, R. Sanfilippo, J. Puig, Q. Yang, L. Mannelli, G. Faa, G. Lanzino, Carotid artery plaque calcifications: Lessons from histopathology to diagnostic imaging. *Stroke* **53**, 290–297 (2022).
58. X. Shi, J. Gao, Q. Lv, H. Cai, F. Wang, R. Ye, X. Liu, Calcification in atherosclerotic plaque vulnerability: Friend or foe? *Front. Physiol.* **11**, 56 (2020).
59. K. Theofilatos, S. Stojkovic, M. Hasman, S. W. van der Laan, F. Baig, J. Barallobre-Barreiro, L. E. Schmidt, S. Yin, X. Yin, S. Burnap, B. Singh, J. Popham, O. Harkot, S. Kampf, M. C. Nackenhorst, A. Strassl, C. Loewe, S. Demyanets, C. Neumayer, M. Bilban, C. Hengstenberg, K. Huber, G. Pasterkamp, J. Wojta, M. Mayr, Proteomic atlas of atherosclerosis: The contribution of proteoglycans to sex differences, plaque phenotypes, and outcomes. *Circ. Res.* **133**, 542–558 (2023).
60. T. R. Sakkers, E. Mili, H. Winter, D. Kapteijn, R. N. Perry, N. Barbera, K. Watts, I. R. Dias, D. Meteva, M. Wesseling, B. M. Mol, G. J. de Borst, D. P. V. de Kleijn, S. W. van der Laan, M. Civelek, S. J. White, L. Maegdefessel, M. Mayr, G. Pasterkamp, M. Mokry, E. D. Benavente, H. M. den Ruijter, Atherosclerotic fibrous plaques in women present ECM remodeling linked to TGF-β. *Circ. Res.* **138**, e327624 (2026).
61. V. Das, S. Narayanan, X. Zhang, O. Bergman, D. Djordjevic, M. Kronqvist, M. Chemaly, G. Karadimou, S. Sundman, I. Prasad, A. J. Buckler, K. C. Knape, N. B. Michaelsen, U. Hedin, L. Matic, Multi-omics data integration from patients with carotid stenosis illuminates key molecular signatures of atherosclerotic instability. *Genome Med.* **18**, 25 (2026).
62. A. Sinha, N. Sachs, E. Kratz, J. Pauli, S. Steigerwald, V. Albrecht, T. Nordmann, E. Ugur, E. H. Rodriguez, M.-L. Engl, P. Skowronek, M. von Scheidt, H. Winter, D. Branzan, H. Schunkert, L. Maegdefessel, M. Mann, Spatially resolved proteomic signatures of atherosclerotic carotid artery disease. medRxiv 2025.02.09.25321955 [Preprint] (2025); https://doi.org/10.1101/2025.02.09.25321955.
63. O. Soehnlein, E. Lutgens, Y. Döring, Distinct inflammatory pathways shape atherosclerosis in different vascular beds. *Eur. Heart J.* **46**, 3261–3272 (2025).
64. E. von Elm, D. G. Altman, M. Egger, S. J. Pocock, P. C. Gøtzsche, J. P. Vandenbroucke, The strengthening the reporting of observational studies in epidemiology (STROBE) statement: Guidelines for reporting observational studies. *Lancet* **370**, 1453–1457 (2007).

65. P. Bankhead, M. B. Loughrey, J. A. Fernández, Y. Dombrowski, D. G. McArt, P. D. Dunne, S. McQuaid, R. T. Gray, L. J. Murray, H. G. Coleman, J. A. James, M. Salto-Tellez, P. W. Hamilton, QuPath: Open source software for digital pathology image analysis. *Sci. Rep.* **7**, 16878 (2017).
66. W. E. Hellings, W. Peeters, F. L. Moll, S. R. D. Piers, J. van Setten, P. J. Van der Spek, J.-P. P. M. de Vries, K. A. Seldenrijk, P. C. De Bruin, A. Vink, E. Velema, D. P. V. de Kleijn, G. Pasterkamp, Composition of carotid atherosclerotic plaque is associated with cardiovascular outcome. *Circulation* **121**, 1941–1950 (2010).
67. L. G. Spagnoli, A. Mauriello, G. Sangiorgi, S. Fratoni, E. Bonanno, R. S. Schwartz, D. G. Piepgras, R. Pistolese, A. Ippoliti, D. R. Holmes, Extracranial thrombotically active carotid plaque as a risk factor for ischemic stroke. *JAMA* **292**, 1845–1852 (2004).
68. A. V. Finn, M. Nakano, J. Narula, F. D. Kolodgie, R. Virmani, Concept of vulnerable/unstable plaque. *Arterioscler. Thromb. Vasc. Biol.* **30**, 1282–1292 (2010).
69. T. Sekimoto, T. Tanaka, T. Shiraki, R. Virmani, A. V. Finn, T. Sekimoto, T. Tanaka, T. Shiraki, R. Virmani, A. V. Finn, T. Sekimoto, T. Tanaka, T. Shiraki, R. Virmani, A. V. Finn, How does atherosclerotic plaque become calcified, and why? *AIMS Med. Sci.* **11**, 421–438 (2024).
70. P. R. Moreno, K.-R. Purushothaman, M. Sirol, A. P. Levy, V. Fuster, Neovascularization in human atherosclerosis. *Circulation* **113**, 2245–2252 (2006).
71. W. J. M. Derksen, W. Peeters, G. W. van Lammeren, C. Tersteeg, J.-P. P. M. de Vries, D. P. V. de Kleijn, F. L. Moll, A. C. van der Wal, G. Pasterkamp, A. Vink, Different stages of intraplaque hemorrhage are associated with different plaque phenotypes: A large histopathological study in 794 carotid and 276 femoral endarterectomy specimens. *Atherosclerosis* **218**, 369–377 (2011).
72. H. S. Bassiouny, H. Davis, N. Massawa, B. L. Gewertz, S. Glagov, C. K. Zarins, Critical carotid stenoses: Morphologic and chemical similarity between symptomatic and asymptomatic plaques. *J. Vasc. Surg.* **9**, 202–212 (1989).
73. Y. Jiang, C. Zhu, W. Peng, A. J. Degnan, L. Chen, X. Wang, Q. Liu, Y. Wang, Z. Xiang, Z. Teng, D. Saloner, J. Lu, Ex-vivo imaging and plaque type classification of intracranial atherosclerotic plaque using high resolution MRI. *Atherosclerosis* **249**, 10–16 (2016).
74. L. H. Bonati, O. Jansen, G. J. de Borst, M. M. Brown, Management of atherosclerotic extracranial carotid artery stenosis. *Lancet Neurol.* **21**, 273–283 (2022).
75. Z. Zhu, W. Yu, Update in the treatment of extracranial atherosclerotic disease for stroke prevention. *Stroke Vasc. Neurol.* **5**, 65–70 (2020).
76. A. Fedorov, R. Beichel, J. Kalpathy-Cramer, J. Finet, J.-C. Fillion-Robin, S. Pujol, C. Bauer, D. Jennings, F. Fennessy, M. Sonka, J. Buatti, S. Aylward, J. V. Miller, S. Pieper, R. Kikinis, 3D Slicer as an image computing platform for the quantitative imaging network. *Magn. Reson. Imaging* **30**, 1323–1341 (2012).
77. M. Wintermark, S. Arora, E. Tong, E. Vittinghoff, B. C. Lau, J. D. Chien, W. P. Dillon, D. Saloner, Carotid plaque computed tomography imaging in stroke and nonstroke patients. *Ann. Neurol.* **64**, 149–157 (2008).
78. S. Achenbach, D. Ropers, U. Hoffmann, B. MacNeill, U. Baum, K. Pohle, T. J. Brady, E. Pomerantsev, J. Ludwig, F. A. Flachskampf, S. Wicky, I.-K. Jang, W. G. Daniel, assessment of coronary remodeling in stenotic and nonstenotic coronary atherosclerotic lesions by multidetector spiral computed tomography. *J. Am. Coll. Cardiol.* **43**, 842–847 (2004).
79. J. Rubin, Q. Cao, Y. Sakai, N. Arnett, H. Q. Phi, A. C. Hu, B. L. Cucchiara, D. Bos, L. Saba, E. Johannson, J. Zee, J. W. Song, Association of carotid plaque calcification attenuation with intraplaque hemorrhage volume: 3D-segmentation analysis. *J. Neuroimaging* **35**, e70071 (2025).
80. A. Kopczak, A. Schindler, A. Bayer-Karpinska, M. L. Koch, D. Sepp, J. Zeller, C. Strecker, J. M. Hempel, C. Yuan, R. Malik, F. A. Wollenweber, T. Boeckh-Behrens, C. C. Cyran, A. Helck, A. Harloff, U. Ziemann, S. Poli, H. Poppert, M. Dichgans, T. Saam, Complicated carotid artery plaques as a cause of cryptogenic stroke. *J. Am. Coll. Cardiol.* **76**, 2212–2222 (2020).
81. A. Bayer-Karpinska, F. Schwarz, F. A. Wollenweber, H. Poppert, T. Boeckh-Behrens, A. Becker, D. A. Clevert, K. Nikolaou, C. Opherk, M. Dichgans, T. Saam, The carotid plaque imaging in acute stroke (CAPIAS) study: Protocol and initial baseline data. *BMC Neurol.* **13**, 201 (2013).
82. C. S. McGinnis, L. M. Murrow, Z. J. Gartner, DoubletFinder: Doublet detection in single-cell RNA sequencing data using artificial nearest neighbors. *Cell Syst.* **8**, 329–337.e4 (2019).
83. R. Fu, A. E. Gillen, R. M. Sheridan, C. Tian, M. Daya, Y. Hao, J. R. Hesselberth, K. A., Riemondy, clustifyr: An R package for automated single-cell RNA sequencing cluster classification. *F1000Res* **9**, 223 (2020).
84. T. Stuart, A. Butler, P. Hoffman, C. Hafemeister, E. Papalexi, W. M. Mauck III, Y. Hao, M. Stoeckius, P. Smibert, R. Satija, Comprehensive integration of single-cell data. *Cell* **177**, 1888–1902.e21 (2019).
85. K. Traeuble, M. Munz, J. Pauli, N. Sachs, E. Vafadarnejad, T. Carrillo-Roa, L. Maegdefessel, P. Kastner, M. Heinig, Integrated single-cell atlas of human atherosclerotic plaques. *Nat. Commun.* **16**, 8255 (2025).
86. R. C. Wirka, D. Wagh, D. T. Paik, M. Pjanic, T. Nguyen, C. L. Miller, R. Kundu, M. Nagao, J. Coller, T. K. Koyano, R. Fong, Y. J. Woo, B. Liu, S. B. Montgomery, J. C. Wu, K. Zhu, R. Chang, M. Alamprese, M. D. Tallquist, J. B. Kim, T. Quertermous, Atheroprotective roles of smooth muscle cell phenotypic modulation and the TCF21 disease gene as revealed by single-cell analysis. *Nat. Med.* **25**, 1280–1289 (2019).
87. K. Börner, S. A. Teichmann, E. M. Quardokus, J. C. Gee, K. Browne, D. Osumi-Sutherland, B. W. Herr II, A. Bueckle, H. Paul, M. Haniffa, L. Jardine, A. Bernard, S.-L. Ding, J. A. Miller, S. Lin, M. K. Halushka, A. Boppana, T. A. Longacre, J. Hickey, Y. Lin, M. T. Valerius, Y. He, G. Pryhuber, X. Sun, M. Jorgensen, A. J. Radtke, C. Wasserfall, F. Ginty, J. Ho, J. Sunshine, R. T. Beuschel, M. Brusko, S. Lee, R. Malhotra, S. Jain, G. Weber, Anatomical structures, cell types and biomarkers of the Human Reference Atlas. *Nat. Cell Biol.* **23**, 1117–1128 (2021).
88. L. Wik, N. Nordberg, J. Broberg, J. Björkesten, E. Assarsson, S. Henriksson, I. Grundberg, E. Pettersson, C. Westerberg, E. Liljeroth, A. Falck, M. Lundberg, Proximity extension assay in combination with next-generation sequencing for high-throughput proteome-wide analysis. *Mol. Cell. Proteomics* **20**, 100168 (2021).

Acknowledgments: We are grateful to all study participants for their contributions to the AtherOMICS biobank. We thank F. M. Boldoczki [Institute for Stroke and Dementia Research (ISD)] for assistance in developing the ex vivo MRI protocol, N. Sachs (Department for Vascular and Endovascular Surgery, TUM Klinikum, Technical University of Munich) for sharing expertise in plaque processing and biobanking, A. Stadie and T. Beer (both ISD) for conducting in vivo MRI scans, and P. Melton and K. Waegemann (both ISD) for assistance in the implementation of the blood biobanking protocol. **Funding:** This work was supported by the German Research Foundation's Emmy Noether Programme GZ GE3461/2-1, ID 512461526 (M.K.G.); Munich Cluster for Systems Neurology (SyNergy) EXC 2145, ID 390857198 (M.K.G.); Fritz Thyssen Foundation Ref. 10.22.2.024 MN (M.K.G.); and Hertie Network of Excellence in Clinical Neuroscience, ID P1230035 (M.K.G.). **Author contributions:** Conceptualization: L.Ž. and M.K.G. Methodology: L.Ž., R.B., J.L., P.V.G.A., A.K., A.S., N.T., and M.K.G. Investigation: L.Ž., R.B., J.L., P.V.G.A., Y.L., L.Z., S.M., A.R., M.A.A., and P.Z. Formal analysis: L.Ž., R.B., J.L., P.V.G.A., Y.L., L.Z., S.M., and A.R. Data curation: L.Ž., R.B., J.L., P.V.G.A., S.M., M.A.A., P.Z., and J.M. Validation: Y.A. Resources: P.R., S.T., L.K., A.M., B.R., M.D., N.T., and M.K.G. Supervision: M.K.G. Funding acquisition: M.K.G. Writing—original draft: L.Ž., R.B., J.L., P.V.G.A., Y.L., L.Z., A.R., M.A.A., and M.K.G. Writing—review and editing: P.Z., A.K., A.S., P.R., Y.A., S.T., L.K., A.M., B.R., M.D., and N.T. **Competing interests:** S.T. received consulting fees from Quanterix unrelated to this work. M.K.G. received consulting fees from Tourmaline Bio Inc., Dexcel Pharma Technologies Ltd., Pheiron GmbH, and Gerson Lehrman Group Inc. unrelated to this work. All other authors declare that they have no competing interests. **Data, code, and materials availability:** All data and code needed to evaluate and reproduce the results are present in the paper and/or the Supplementary Materials. The biomaterials and deidentified datasets from the AtherOMICS biobank, including data underlying the pilot results presented in this study, are available upon submission of a research proposal, subject to scientific review and completion of a material transfer agreement through LMU Klinikum. Research proposals should be submitted to Forschung.ISD@med.uni-muenchen.de. The code underlying the analyses in this publication can be accessed under the following DOI: 10.5281/zenodo.21837251.

Submitted 9 December 2025
Accepted 19 August 2026
Published 25 September 2026
10.1126/sciadv.aee2639